ARTICLE

Expansion of MAIT cells in the combined absence of NKT and γδ-T cells

Calvin Xu [1], Shihan Li [1], Thomas S Fulford [1], Susan N Christo [1], Laura K Mackay [1], Daniel HD Gray [2,3], Adam P Uldrich [1], Daniel G Pellicci [1,4,5,✉], Dale I Godfrey [1,✉] and Hui-Fern Koay [1,✉]

Mucosal-associated invariant T (MAIT) cells, natural killer T (NKT) cells, and γδT cells are collectively referred to as 'unconventional T cells' due to their recognition of non-peptide antigens and restriction to MHC-I-like molecules. However, the factors controlling their widely variable frequencies between individuals and organs are poorly understood. We demonstrated that MAIT cells are increased in NKT or γδT cell-deficient mice and highly expand in mice lacking both cell types. TCRα repertoire analysis of γδT cell-deficient thymocytes revealed altered *Trav* segment usage relative to wild-type thymocytes, highlighting retention of the *Tcra-Tcrd* locus from the 129 mouse strain used to generate *Tcrd*$^{-/-}$ mice. This resulted in a moderate increase in distal *Trav* segment usage, including *Trav1*, potentially contributing to increased generation of *Trav1-Traj33*$^{+}$ MAIT cells in the *Tcrd*$^{-/-}$ thymus. Importantly, adoptively transferred MAIT cells underwent increased homeostatic proliferation within NKT/gdT cell-deficient tissues, with MAIT cell subsets exhibiting tissue-specific homing patterns. Our data reveal a shared niche for unconventional T cells, where competition for common factors may be exploited to collectively modulate these cells in the immune response. Lastly, our findings emphasise careful assessment of studies using NKT or γδT cell-deficient mice when investigating the role of unconventional T cells in disease.

Mucosal Immunology (2023) 16:446–461; https://doi.org/10.1016/j.mucimm.2023.05.003

INTRODUCTION

Unconventional T cells comprise distinct T-cell lineages that recognize non-peptide antigens and are implicated in modulating the immune response in a myriad of contexts, ranging from infection, cancer, autoimmunity, and wound healing[1,2]. These lineages comprise populations such as MR1-restricted mucosal-associated invariant T (MAIT) cells and clusters of differentiation (CD1d)-restricted type I 'invariant' natural killer T (NKT) cells, both of which are characterized by their constrained αβTCR repertoires. Briefly, the MAIT-TCRα chain, *Trav1-Traj33* (Vα19-Jα33), is used by nearly all mouse MAIT cells, while *Trav11-Traj18* (Vα14-Jα18) forms the TCRα chain for most type I NKT cells. The expression of a *Trav1-Traj33*$^{+}$ or *Trav11-Traj18*$^{+}$ TCR by MAIT and NKT cells, respectively, imbues these cells with their unique antigen specificity and function. MAIT cells recognize vitamin B metabolite-derived antigens, such as 5-(2-oxopropylideneamino)-6-$_{D}$-ribitylaminouracil (5-OP-RU), presented by MR1[3], whereas NKT cells recognize glycolipid antigens, such as α-galactosylceramide (α-GalCer), presented in the context of CD1d[1]. In addition, other unconventional T-cell subsets which express more diverse αβ or γδTCR repertoires include type II NKT cells, intraepithelial lymphocytes (IELs), and CD4^{-}CD8^{-} double negative (DN) T-cell subsets, and gamma delta T (γδT) cells[1,4–6]. In some ways, γδT cells are the most distinct as they express a γδTCR encoded by *Trgv* and *Trdv* gene segments and exhibit a broad range of antigen specificities[1,7,8].

Unconventional T-cell frequencies vary widely between human individuals and in different mouse strains, however, the mechanisms that control this variation and their development, are not well-understood. Like conventional T cells, commitment to the MAIT, NKT, or γδT-cell lineages occurs in the thymus and is initiated after successful TCR rearrangement and expression within developing thymocytes. TCRβ, TCRγ, and TCRδ chain rearrangement occurs during the CD4^{-}CD8^{-} DN thymocyte stage of development, whereby expression of a productive γδTCR over a TCRβ chain, in addition to strong TCR signaling through the γδTCR heterodimer, leads to commitment to the γδT-cell lineage[9]. In contrast, successful rearrangement of a TCRβ chain and weaker signaling through the pre-TCR on DN thymocytes leads to αβT lineage commitment, transition to the CD4^{+}CD8^{+} double positive (DP) thymocyte stage, and eventual TCRα chain rearrangement[9]. Importantly, expression of the invariant *Trav1-Traj33*$^{+}$ MAIT- or *Trav11-Traj18*$^{+}$ NKT-TCR, endows developing DP thymocytes with the ability to recognize their

[1]Department of Microbiology and Immunology at the Peter Doherty Institute for Infection and Immunity, The University of Melbourne, Parkville, Australia. [2]Walter and Eliza Hall Institute of Medical Research, Parkville, Australia. [3]Department of Medical Biology, University of Melbourne, Parkville, Australia. [4]Murdoch Children's Research Institute, Melbourne, Australia. [5]Department of Paediatrics, University of Melbourne, Parkville, Australia. ✉ email: dan.pellicci@mcri.edu.au; godfrey@unimelb.edu.au; hf.koay@unimelb.edu.au

Received: 3 March 2023 Accepted 3 May 2023
Published online: 13 May 2023

restricting elements, MR1 or CD1d, respectively, leading to positive selection and commitment to the MAIT or NKT-cell lineages[10–13].

The development of MAIT, NKT, and subsets of γδT cells is regulated by a number of common mechanisms[8], most notably, the SLAM-SAP-FYN pathway[14–17], and the transcription factor promyelocytic leukemia zinc finger (PLZF)[18–21]. Additionally, these cells polarize into distinct functional subsets later in development as defined by the expression of key transcription factors. Namely, RORγt-expressing MAIT, NKT, and γδT cells are characterized by their production of IL-17A, while those that express T-bet potently produce interferon (IFN)-γ. Likewise, the expression of GATA-3 by subsets of NKT and γδT cells governs their production of IL-4. This functional diversification of developing unconventional T cells occurs after expression of PLZF and is also underpinned by the acquisition of common transcriptomic signatures shared by mouse unconventional T cells, as revealed by RNA sequencing[22–26].

We previously reported that MAIT cells are increased in NKT cell-deficient *Cd1d*$^{-/-}$ mouse models[19] and recent studies have described an increase in MAIT cells in γδT cell-deficient *Tcrd*$^{-/-}$ mice[23,27,28], suggesting a compensatory niche shared by these cells. However, the mechanisms driving increased levels of MAIT cells in *Cd1d*$^{-/-}$ and *Tcrd*$^{-/-}$ mice have not been clearly defined. Interleukin (IL)-7 and IL-15, which are known for their role in conventional T-cell homeostasis[29], have been also strongly implicated in the homeostatic regulation of unconventional T cells[30–34]. It is also unclear whether competition for shared factors is the only contributing mechanism governing the expansion of MAIT cells in *Cd1d*$^{-/-}$ and *Tcrd*$^{-/-}$ mice and whether the absence of both NKT cells and γδT cells would further make space in the unconventional T-cell niche, leading to a greater abundance of MAIT cells.

Using *Cd1d*$^{-/-}$ and *Tcrd*$^{-/-}$ mouse models we show that MAIT cells are increased in both thymic and peripheral tissues, and most importantly, that these increases were markedly augmented in *Cd1d*$^{-/-}$*Tcrd*$^{-/-}$ double-deficient mice. We also report an increase in MAIT-TCRα chain rearrangement within developing thymocytes from *Tcrd*$^{-/-}$ and *Cd1d*$^{-/-}$*Tcrd*$^{-/-}$ mice and demonstrate that in the absence of NKT and γδT cells, MAIT cells have a greater proliferative capacity. Accordingly, our study highlights a shared unconventional T-cell niche, which has important implications for targeting multiple unconventional T-cell lineages in disease settings.

RESULTS

MAIT cells expand in the absence of NKT cells

We have previously established that MAIT cells are expanded in *Cd1d*$^{-/-}$ mice, most profoundly when on the BALB/c background[19]. To determine if this was due to the loss of NKT cells in these mice, we sought to compare MAIT cells in *Cd1d*$^{-/-}$ mice to those in *Traj18*-deficient mice (*Traj18*$^{-/-}$) which lack type I (*Trav11-Traj18*$^{+}$) NKT cells but retain other CD1d-restricted (type II) NKT cells as well as CD1d. As a previous *Traj18*$^{-/-}$ mouse strain exhibited a severely constrained *Traj* gene segment usage[35], we generated a new BALB/c *Traj18*$^{-/-}$ mouse strain that, other than the specific loss of *Traj18*, has a replete *Traj* repertoire (Supplementary Fig. 1A). We confirmed that our BALB/c *Traj18*$^{-/-}$ mice lack type I NKT cells, as expected (Supplementary Fig. 1B). MAIT cells were examined in BALB/c wild-type (WT), *Traj18* heterozygous ($^{+/-}$), *Traj18*$^{-/-}$, and *Cd1d*$^{-/-}$ mice. The frequency of MAIT cells was significantly increased in the thymus, spleen, inguinal lymph nodes (iLNs), and liver of BALB/c *Traj18*$^{-/-}$ mice relative to BALB/c WT controls, although MAIT cell numbers were only significantly increased in the thymus of *Traj18*$^{-/-}$ mice (Figs. 1A and 1C). No significant difference in MAIT cell frequency or numbers was detected in BALB/c *Traj18*$^{+/-}$ mice in any tissue. In contrast, the frequency and number of MAIT cells was significantly increased in BALB/c *Cd1d*$^{-/-}$ mice in all organs examined (Figs. 1A and 1C) and there was also an increase in the frequency and number of liver MAIT cells when comparing BALB/c *Cd1d*$^{-/-}$ to *Traj18*$^{-/-}$ mice. As we have previously published[19], an increase, albeit less dramatic, in MAIT cells was also observed in C57BL/6 *Cd1d*$^{-/-}$ mice relative to C57BL/6 WT mice. Within the C57BL/6 strains, we observed an increase in MAIT cell frequency in the liver, and in total MAIT cell numbers in the thymus and spleen of C57BL/6 *Cd1d*$^{-/-}$ compared to C57BL/6 WT mice (Figs. 1B and 1D). Collectively, these data imply that observed increases in MAIT cells in *Cd1d*$^{-/-}$ mice (Fig. 1) are likely due to the loss of type I NKT cells as increases in MAIT cells were observed in both *Traj18*$^{-/-}$ and *Cd1d*$^{-/-}$ mouse models. However, as some of the increases were more profound in the *Cd1d*$^{-/-}$ mice compared to the *Traj18*$^{-/-}$ mice, this suggests that type II NKT cells may also occupy the same niche. Unfortunately, we have no way to specifically deplete type II NKT cells to test this hypothesis.

We next investigated whether the loss of NKT cells impacted γδT cell numbers in a similar manner. The absolute number of γδT cells was significantly increased in the thymus of *Traj18*$^{-/-}$ mice compared to BALB/c WT controls (Supplementary Figs. 1C, E). Interestingly, the frequency and number of γδT cells were significantly higher in the thymus of BALB/c *Cd1d*$^{-/-}$ mice but not in C57BL/6 *Cd1d*$^{-/-}$ mice compared to WT controls (Supplementary Figs. 1C–F). The frequency of γδT cells was also significantly increased in livers of both BALB/c and C57BL/6 *Cd1d*$^{-/-}$ mice and in the iLNs of BALB/c but not C57BL/6 *Cd1d*$^{-/-}$ mice relative to their corresponding WT controls. However, increases in γδT cell frequency did not necessarily correspond with significant differences in total γδT cell numbers (Supplementary Figs. 1C–F). These data suggest that both MAIT and, to a lesser extent, γδT cell frequencies are suppressed in the presence of NKT cells. Lastly, differences between NKT cell-deficient C57BL/6 and BALB/c mouse models also highlight strain-specific variation within unconventional T cell compartments and associated niches.

Expansion of MAIT cells in γδT cell-deficient mice is compounded by the loss of NKT cells

In line with emerging reports that show an increase in MAIT cell frequencies in the skin[27] and thymus[23] of C57BL/6 *Tcrd*$^{-/-}$ mice, we report that MAIT cells are significantly and systemically increased in both frequency and number in the thymus, spleen, liver, and iLNs of C57BL/6 *Tcrd*$^{-/-}$ mice relative to WT controls, as well as in the gut, lungs, and mesenteric LNs (Figs. 2A and 2B and Supplementary Fig. 2A). Furthermore, we also observed a moderate increase in NKT cell frequencies in the thymus, spleen, liver, and iLNs of C57BL/6 *Tcrd*$^{-/-}$ mice, however, total NKT cell numbers did not reach statistical significance (Supplementary Figs. 2C–D, 3A–B). In addition, there were no changes observed in NKT and γδT cells in C57BL/6 *Mr1*$^{-/-}$ mouse organs, apart from an increase in the proportion of γδT cells in *Mr1*$^{-/-}$ iLNs (Supplementary Fig. 2E). Thus, these data suggest that MAIT cells are expanded in mice that lack γδT cells, providing further evidence for an interplay between MAIT and γδT cells.

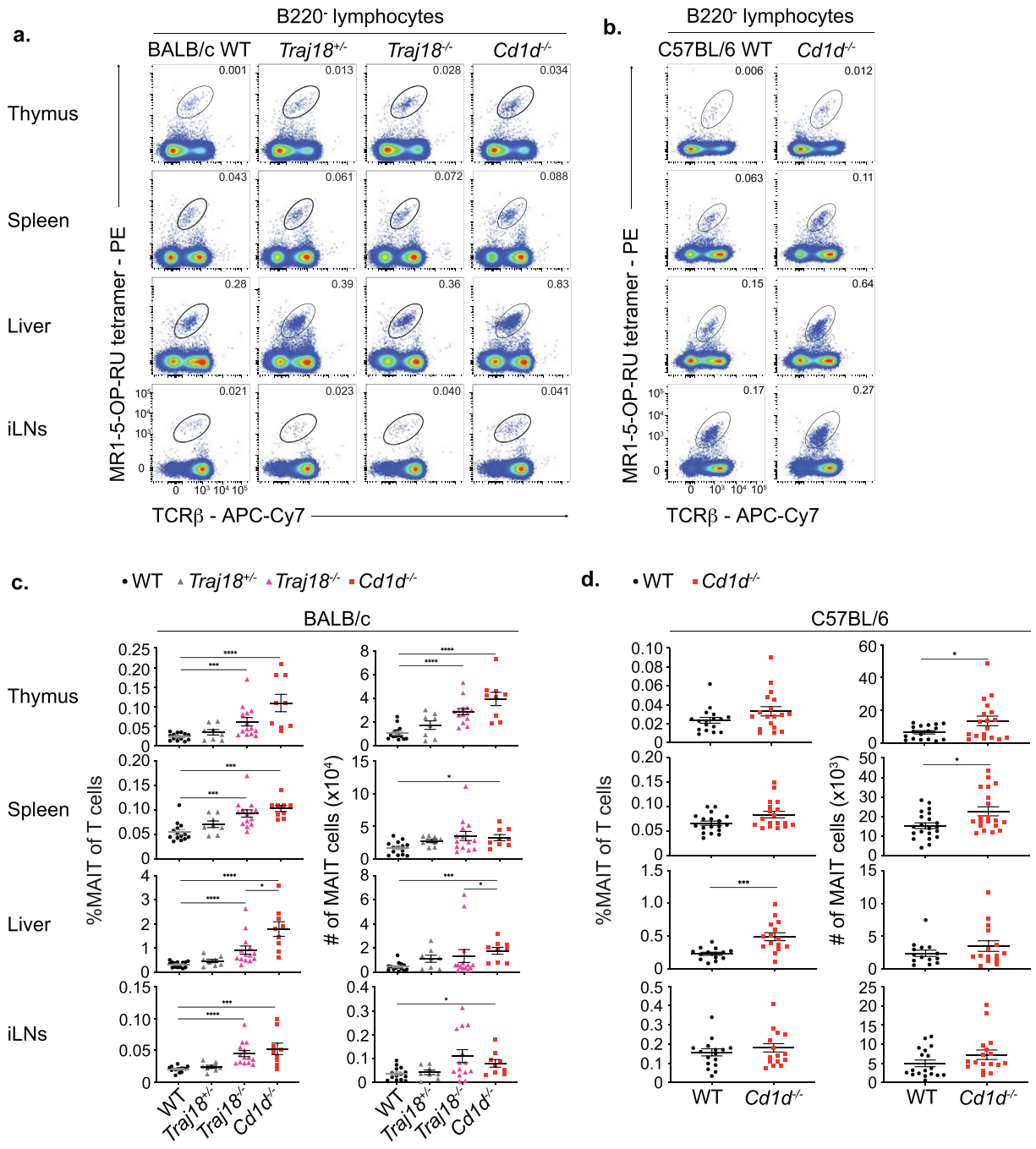

Fig. 1 MAIT cell frequencies increase systemically in the absence of NKT cells. (A & B) Flow cytometry analysis of TCRβ$^+$ MR1-5-OP-RU tetramer$^+$ MAIT cells from thymus, spleen, liver, and iLNs of WT, *Traj18*$^{+/-}$, *Traj18*$^{-/-}$, and *Cd1d*$^{-/-}$ mice of the BALB/c background (A) and of WT and *Cd1d*$^{-/-}$ mice of the C57BL/6 background (B). Plots were pre-gated on B220$^-$ lymphocytes. Numbers within fluorescence activated cell sorting (FACS) plots represent percentage of gated MAIT cells out of B220$^-$ lymphocytes. (C & D) Graphs depict MAIT cell frequency as a percentage of all T cells (αβ and γδT cells) and absolute number from specified organs. Horizontal bars depict mean ± standard error of the mean. Each symbol represents an individual mouse, a total of 9–14 mice in the BALB/c WT, *Traj18*$^{+/-}$, *Traj18*$^{-/-}$, and *Cd1d*$^{-/-}$ groups were examined across five independent experiments (C), and a total of 14–18 mice for C57BL/6 WT and *Cd1d*$^{-/-}$ across six independent experiments. (D) * $p \leq 0.05$, ** $p \leq 0.01$, *** $p \leq 0.001$, **** $p \leq 0.0001$ for (C) using a Mann-Whitney U test with a Bonferroni correction for three hypotheses and (D) using a Mann-Whitney U test. αβ = alpha-beta; APC = Allophycocyanin; CD = clusters of differentiation; γδT = gamma-delta T; iLNs = inguinal lymph nodes; MAIT = mucosal-associated invariant T cell; NKT = natural killer T cells; PE= Phycoerythrin; TCR = T cell receptor; WT = wild-type.

We next generated C57BL/6 *Cd1d*$^{-/-}$*Tcrd*$^{-/-}$ mice to investigate whether the absence of both NKT and γδT cells would drive a further expansion of MAIT cells. In all organs examined, *Cd1d*$^{-/-}$*Tcrd*$^{-/-}$ mice displayed similar cellularity to that of WT mice in terms of absolute number of lymphocytes and total T cells, with the exception of the liver (Supplementary Figs. 3C, D). The

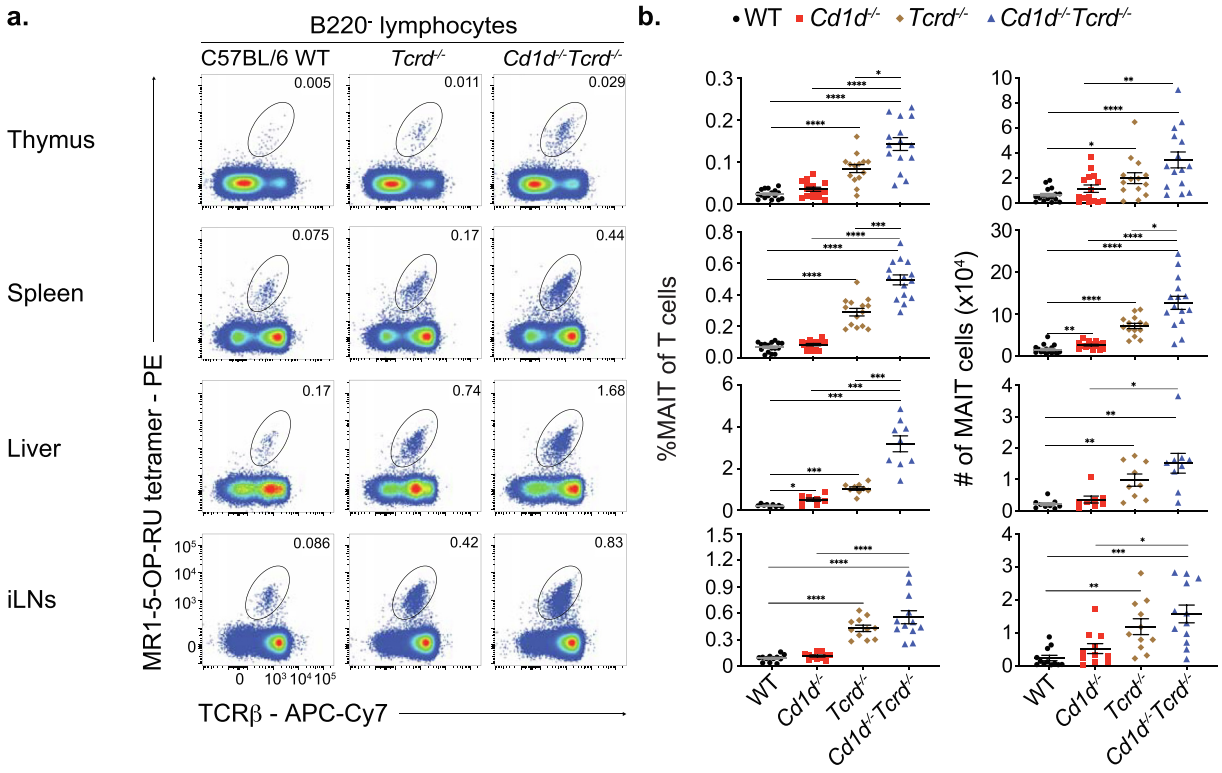

Fig. 2 MAIT cells increase in the absence of γδT cells and dramatically expand in the absence of both γδT and NKT cells. (A) Flow cytometry analysis of TCRβ$^+$ MR1-5-OP-RU tetramer$^+$ MAIT cells from thymus, spleen, liver, and iLNs of C57BL/6 WT, *Tcrd*$^{-/-}$ and *Cd1d*$^{-/-}$*Tcrd*$^{-/-}$ mice. Plots were pre-gated on B220$^-$ lymphocytes. Numbers within FACS plots represent frequency of gated MAIT cells out of B220$^-$ lymphocytes. (B) MAIT cell frequency as a percentage of all T cells (αβ and γδT cells) and absolute number within indicated organs from WT, *Cd1d*$^{-/-}$, *Tcrd*$^{-/-}$, and *Cd1d*$^{-/-}$*Tcrd*$^{-/-}$ mice were analyzed on the same day and graphed. Horizontal bars represent mean ± standard error of the mean. Each symbol represents an individual mouse, with a total of 9–23 mice in each group across 4–7 independent experiments. * $p \leq 0.05$, ** $p \leq 0.01$, *** $p \leq 0.001$, **** $p \leq 0.0001$ using a Mann-Whitney U test with a Bonferroni correction for five hypotheses. αβ = alpha-beta; γδT = gamma-delta T; iLNs = inguinal lymph nodes; MAIT = mucosal-associated invariant T cell; NKT = natural killer T cells; TCR = T cell receptor; WT = wild-type.

decrease in T cell numbers in the *Cd1d*$^{-/-}$*Tcrd*$^{-/-}$ liver (Supplementary Figs. 3C, D), likely reflected the loss of both NKT and γδT cells which collectively make up to 50% of T cells in the liver. In addition, the frequency and numbers of non-MAIT/NKT/γδT conventional CD4$^+$ and CD8$^+$ αβT cells were unchanged between WT and *Cd1d*$^{-/-}$*Tcrd*$^{-/-}$ mice at the steady state (Supplementary Fig. 3D). CD4$^-$CD8$^-$ DN αβT cells, which are poorly characterized and may contain other unconventional T cell subsets, were relatively rare and were only significantly increased in both frequency and number within the iLNs of *Cd1d*$^{-/-}$*Tcrd*$^{-/-}$ mice (Supplementary Fig. 3D). Furthermore, the frequency of PLZF$^+$ non-MAIT/NKT/γδT αβT cells were not increased within the thymus, spleen, liver, and iLNs of *Cd1d*$^{-/-}$*Tcrd*$^{-/-}$ mice (Supplementary Fig. 3E).

Simultaneous analysis of WT, *Cd1d*$^{-/-}$, *Tcrd*$^{-/-}$, and *Cd1d*$^{-/-}$*Tcrd*$^{-/-}$ mice revealed that MAIT cells levels are highly and significantly increased in *Cd1d*$^{-/-}$*Tcrd*$^{-/-}$ mice relative to C57BL/6 WT controls in all organs examined and that *Cd1d*$^{-/-}$*Tcrd*$^{-/-}$ MAIT cells levels often were higher than that in *Cd1d*$^{-/-}$ and *Tcrd*$^{-/-}$ mice (Fig. 2B). In addition, the extent to which MAIT cells were increased in *Cd1d*$^{-/-}$*Tcrd*$^{-/-}$ mice varied between the tissues examined, ranging from a 6 to 14-fold increase in frequency and a 5 to 8-fold increase in number (Figs. 2A and 2B). Additionally, the frequency of MAIT cells in the thymus, spleen, and liver of *Cd1d*$^{-/-}$*Tcrd*$^{-/-}$ mice was significantly increased relative to corresponding *Tcrd*$^{-/-}$ organs, and though absolute MAIT cell numbers trended higher in all organs, only increases in the spleen reached statistical significance between *Tcrd*$^{-/-}$ and *Cd1d*$^{-/-}$*Tcrd*$^{-/-}$mice. MAIT cell levels were also significantly increased in frequency and number in *Cd1d*$^{-/-}$*Tcrd*$^{-/-}$ mice compared to *Cd1d*$^{-/-}$ mice (Figs. 2A and 2B). Accordingly, these data imply that the combined loss of both NKT and γδT cells leads to a large expansion of MAIT cells in *Cd1d*$^{-/-}$*Tcrd*$^{-/-}$ mice.

Expanded MAIT cells are unaltered in phenotypic and functional subset distribution

We next explored whether the expansion of MAIT cells was preferentially skewed to a specific subpopulation, based on the expression of surface markers and the transcription factors RORγt, T-bet, and PLZF. We observed that the overall CD4/CD8 co-receptor expression of MAIT cells was similar between each mouse strain examined, with some subtle but significant changes. For example, the frequency of CD8$^+$ MAIT cells was significantly increased in the liver of *Cd1d*$^{-/-}$ mice relative to WT controls (Fig. 3A, Supplementary Fig. 4A), while in contrast, the frequency of CD8$^+$ MAIT cells was significantly decreased within the spleen, liver, and iLNs of *Tcrd*$^{-/-}$ mice, and the spleen of *Cd1d*$^{-/-}$*Tcrd*$^{-/-}$ mice, compared to corresponding WT organs (Fig. 3A, Supplementary Fig. 4A). CD4$^-$CD8$^-$ DN MAIT cells were significantly increased in the spleens of *Cd1d*$^{-/-}$*Tcrd*$^{-/-}$ mice

relative to WT controls. (Fig. 3A, Supplementary Fig. 4A). All MAIT cells in these organs expressed similar levels of the effector memory marker, CD44, and the transcription factor, PLZF (Fig. 3B).

In the steady state, unconventional T cell populations can be divided into mutually exclusive functional subsets defined by expression of RORγt and T-bet[19,23,25,36,37]. Generally, RORγt-expressing MAIT-17, NKT-17, and CD44^{hi} γδT-17 cells, predominate in the lymph nodes, in contrast to the liver in which T-bet-expressing MAIT-1, NKT-1, and CD44^{hi} γδT-1 cells, are enriched. Regardless, these functionally distinct MAIT cell subsets were present within thymus, spleen, liver, and iLNs of all mouse strains examined (Fig. 3A, Supplementary Fig. 4A). Moreover, the tissue-specific distributions of T-bet^{+} MAIT-1 and RORγt^{+} MAIT-17 cells were overall similar in *Cd1d*$^{-/-}$, *Tcrd*$^{-/-}$, and *Cd1d*$^{-/-}$*Tcrd*$^{-/-}$ mice compared to WT mice. Likewise, NKT

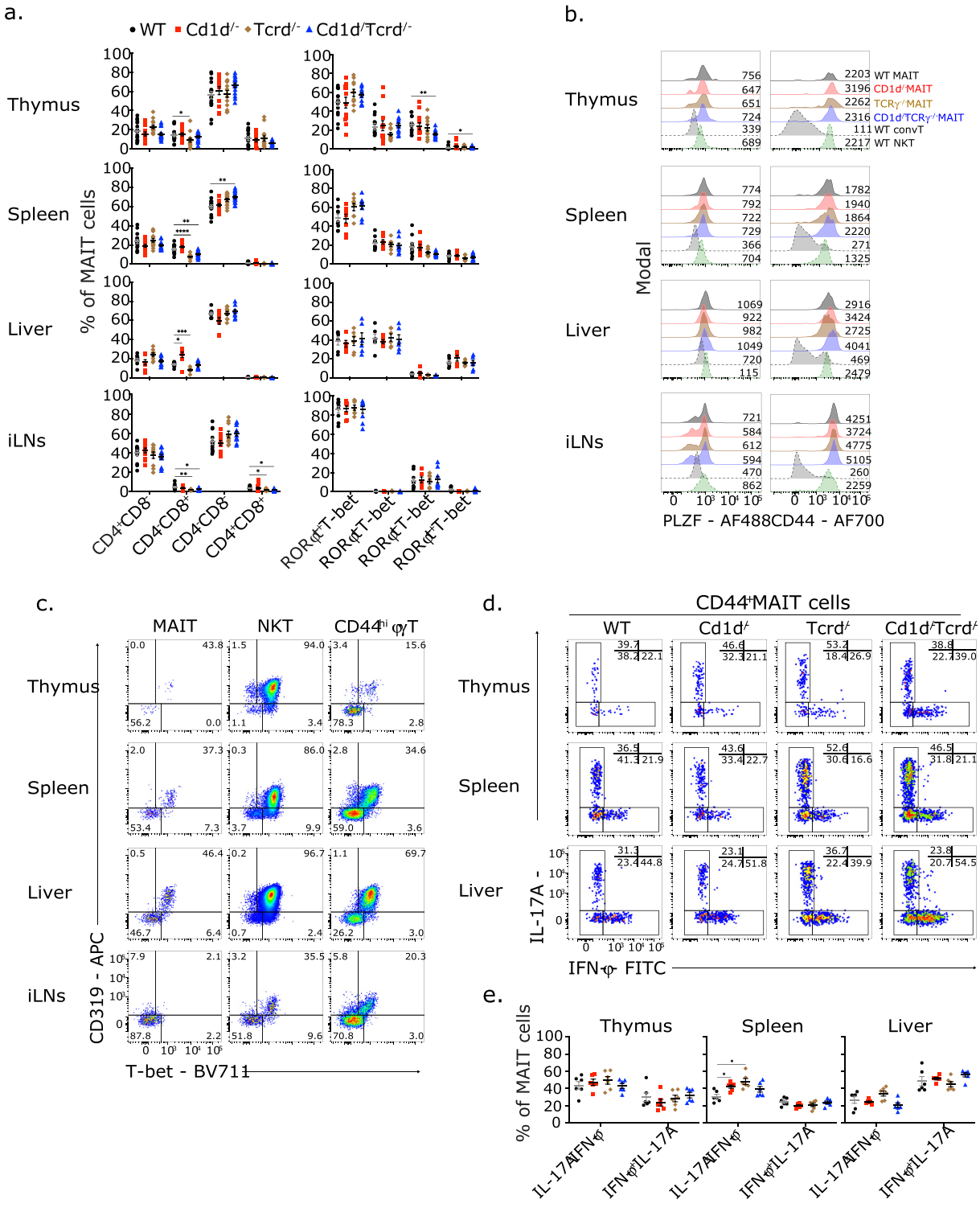

and γδT cell functional and CD4/8 co-receptor subsets were similar within *Tcrd*$^{-/-}$ and *Cd1d*$^{-/-}$ mice, respectively, relative to WT controls (Supplementary Fig. 5). Interestingly, in all mouse strains, ∼10-15% of liver MAIT cells co-expressed RORγt and T-bet (Fig. 3A, Supplementary Fig. 4A), a subset previously undetected at the steady state[33]. We previously reported that the MAIT-1 and MAIT-17 functional subsets can be respectively distinguished via the surface markers CD319 and CD138 or ICOS[17]. Analysis of these markers on other unconventional T cell populations from the thymus, spleen, liver, and iLNs showed that CD319 was a marker of T-bet^{+} MAIT-1, NKT-1 and γδT-1 cells (Fig. 3C). In contrast, though CD138 and ICOS reliably marked MAIT-17 and NKT-17 cells[17,38] across all tissues examined, they were less reliable for identifying γδT-17 cells (Supplementary Figs. 4B, C).

The similar distribution of MAIT cell functional subsets across these mouse models was further reflected in the respective capacities of MAIT-17 and MAIT-1 cells to produce IL-17A and IFN-γ. After PMA and ionomycin stimulation, the proportions of IL-17A- and IFN-γ-producing MAIT cells were similar in the thymus, spleen, and liver of *Cd1d*$^{-/-}$, *Tcrd*$^{-/-}$, and *Cd1d*$^{-/-}$*Tcrd*$^{-/-}$ mice relative to WT controls, though the increase in IL-17A^{+} MAIT cells in the *Cd1d*$^{-/-}$ and *Tcrd*$^{-/-}$ spleens relative to the WT spleen was significant (Figs. 3D and 3E). Despite the detection of RORγt^{+}T-bet^{+} MAIT cells in the liver (Fig. 3A, Supplementary Fig. 4A), MAIT cells that produced both IFN-γ and IL-17A were not detected (Figs. 3D and 3E). Moreover, the frequencies of IL-17A and IFN-γ-producing NKT cells within *Tcrd*$^{-/-}$ mice and CD44^{+} γδT cells in *Cd1d*$^{-/-}$ mice when compared to their counterparts in WT mice were similar (Supplementary Fig. 4D). In terms of TCRβ chains preferentially used by mouse MAIT cells[36], small differences in the frequency of Vβ8.1/2^{+} spleen MAIT cells were observed between WT and *Cd1d*$^{-/-}$*Tcrd*$^{-/-}$ mice, but the overall preferential usage of Vβ8 over Vβ6 was similar (Supplementary Fig. 4E). Furthermore, the expression of CD127 and CD122 by MAIT cells from *Cd1d*$^{-/-}$*Tcrd*$^{-/-}$ mice was similar to that of MAIT cells from WT mice (Supplementary Fig. 4F). In addition, the levels of *Il-7* and *Il-15* mRNA transcripts within the thymus, spleen, liver, and iLNs were similar between WT and *Cd1d*$^{-/-}$*Tcrd*$^{-/-}$ mice, as measured by quantitative polymerase chain reaction (qPCR) (Supplementary Fig. 5E). Overall, these results demonstrate that the expansion of MAIT cells in the mouse models of interest, and to a lesser extent, NKT and γδT cells in *Tcrd*$^{-/-}$ and *Cd1d*$^{-/-}$ mice, respectively, was not confined to any phenotypic or functional subset.

MAIT-TCRα chain rearrangements are increased in *Tcrd*$^{-/-}$ and *Cd1d*$^{-/-}$*Tcrd*$^{-/-}$ mice

As thymic MAIT cells were increased in *Cd1d*$^{-/-}$, *Tcrd*$^{-/-}$ and *Cd1d*$^{-/-}$*Tcrd*$^{-/-}$ mice, we examined the surface expression of MR1 on DP thymocytes and found that MR1 levels were ubiquitously low and similar on WT and *Cd1d*$^{-/-}$*Tcrd*$^{-/-}$, and WT and *Tcrd*$^{-/-}$ thymocytes (Supplementary Figs. 5C, D). Thus, we hypothesized that altered dynamics of TCRα rearrangement within these strains may influence the rearrangement of the *Trav1-Traj33* MAIT-TCRα chain within developing thymocytes. Notably, *Tcrd*$^{-/-}$ mice were generated via the genetic disruption of the *Trdc* gene segment[39] which is located within the *Tcra-Tcrd* locus on chromosome 14[40]. Here, TCRδ gene segments are interspersed among TCRα segments, where *Trdc* is situated between the arrays of upstream *Trav/Trdv* and downstream *Traj* gene segments (Supplementary Fig. 6A[40]).

We first analyzed *Trav1-Traj33* transcript levels within immature CD4^{+}CD8^{+}TCRβ$^{neg/int}$ DP thymocytes by qPCR, removing contamination by expanded thymic MAIT and NKT cells by sorting on MR1-5-OP-RU-tetramer-negative and CD1d-α-GalCer-tetramer-negative thymocytes. The expression of *Trav1-Traj33* transcripts within DP thymocytes from *Tcrd*$^{-/-}$ and *Cd1d*$^{-/-}$*Tcrd*$^{-/-}$ mice relative to WT controls were, on average, increased ∼2-fold (Fig. 4A, left), regardless of additional standardization to *Trac* transcripts (Fig. 4A, right). However, *Trav1-Traj33* transcripts were similar in *Cd1d*$^{-/-}$ thymocytes relative to WT controls, and, as expected, the abundance of the *Trav11-Traj18* NKT-TCRα chain, in DP thymocytes from *Cd1d*$^{-/-}$, *Tcrd*$^{-/-}$ and *Cd1d*$^{-/-}$*Tcrd*$^{-/-}$ mice was unchanged compared to WT controls (Fig. 4A). We also found that *Trac* transcript levels were similar in *Cd1d*$^{-/-}$, *Tcrd*$^{-/-}$ and *Cd1d*$^{-/-}$*Tcrd*$^{-/-}$ thymocytes relative to WT thymocytes, reinforcing that increases in *Trav1-Traj33*$^{+}$ MAIT-TCRα chain transcripts were not due increases in overall TCRα gene rearrangements (Fig. 4A). Thus, our data suggests a potential bias toward usage of *Trav* gene segments most distal to the *Traj* locus, such as *Trav1* which is located at the 5′ end of the *Trav/Trdv* array, but not of more 3′-located, *Traj*-proximal gene segments, such as *Trav11,* during TCRα rearrangement within DP thymocytes from *Tcrd*$^{-/-}$ but not *Cd1d*$^{-/-}$ mice.

TCRα chain usage and corresponding αβT cell repertoire are altered in *Tcrd*$^{-/-}$ mice

To enable a more in-depth analysis and expand upon our previous findings (Fig. 4), we profiled the TCRα repertoire of C57BL/6 WT and *Tcrd*$^{-/-}$ mice using a 5′RACE-based deep sequencing

Fig. 3 Phenotype of MAIT cells is unchanged in WT, *Cd1d*$^{-/-}$, *Tcrd*$^{-/-}$, and *Cd1d*$^{-/-}$*Tcrd*$^{-/-}$ mice. (A) Proportions of CD4/CD8 and RORγt/T-bet MAIT cell subsets were graphed. Horizontal lines represent mean ± standard error of the mean. A total of 5–16 mice were in each group across 2–5 independent experiments. * $p \leq 0.05$, ** $p \leq 0.01$, *** $p \leq 0.001$, **** $p \leq 0.0001$ using a Mann-Whitney U test with a Bonferroni correction for three hypotheses. (B) Representative overlay histograms of PLZF (left column) and CD44 (right column) expression of MAIT cells within indicated organs from WT (black), *Cd1d*$^{-/-}$ (red), *Tcrd*$^{-/-}$ (brown), *Cd1d*$^{-/-}$*Tcrd*$^{-/-}$ (blue) mice. PLZF and CD44 expression of WT conventional T cells (gray, dotted line) and NKT cells (green, dotted line) were included for comparison. A total of 6–9 mice were in each group across 2–3 independent experiments. (C) Flow cytometry analysis of CD319 and T-bet expression by MAIT, NKT, and CD44^{+} γδT cells in C57BL/6 mice as indicated. (D) IL-17A and IFN-γ expression by CD44^{+} MAIT cells from specified organs in mouse strains as indicated, post-PMA and ionomycin stimulation for 4 hours. Numbers within FACS plots represent frequency of gated cells out of all MAIT cells. (E) Proportions of IL-17A- and IFN-γ-producing MAIT cells were graphed. Horizontal lines represent mean ± standard error of the mean. Each symbol represents an individual mouse. A total of six mice were in each group and were analysed across two independent experiments. * $p \leq 0.05$ using a Mann-Whitney U test with a Bonferroni correction for three hypotheses. CD = clusters of differentiation; IFN= interferon; IL = interleukin; iLNs = inguinal lymph nodes; MAIT = mucosal-associated invariant T cell; NKT = natural killer T cells; PLZF = promyelocytic leukemia zinc finger; TCR = T cell receptor; WT = wild-type.

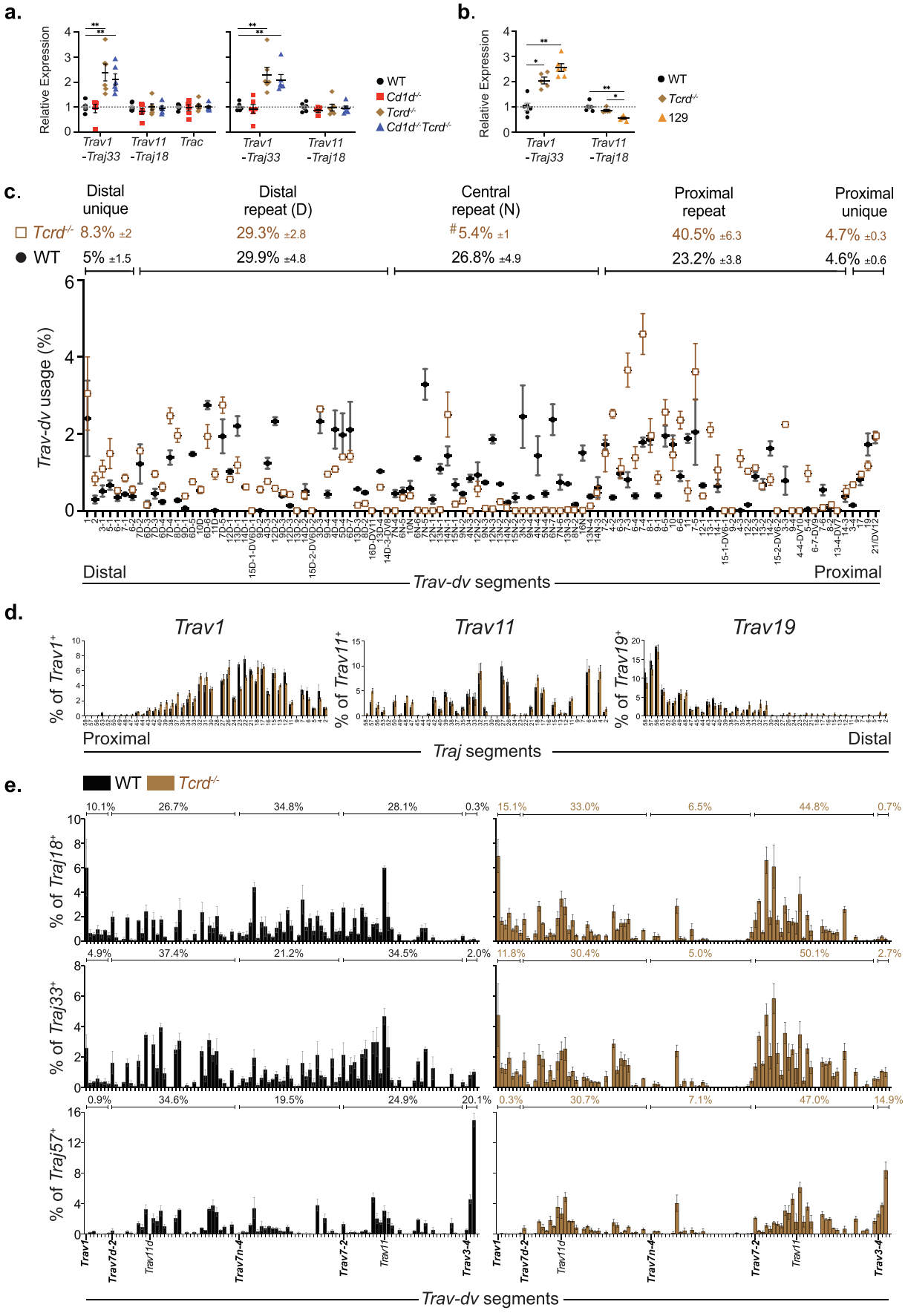
a.
Relative Expression
Trav1 -Traj33
Trav11 -Traj18
Trac
WT
Cd1d-/-
Tcrd-/-
Cd1d-/-Tcrd-/-
b.
Relative Expression
Trav1 -Traj33
Trav11 -Traj18
WT
Tcrd-/-
129
c.
Distal unique
Distal repeat (D)
Central repeat (N)
Proximal repeat
Proximal unique
Tcrd-/- 8.3% ±2
29.3% ±2.8
#5.4% ±1
40.5% ±6.3
4.7% ±0.3
WT 5% ±1.5
29.9% ±4.8
26.8% ±4.9
23.2% ±3.8
4.6% ±0.6
Trav-dv usage (%)
Distal
Trav-dv segments
Proximal
d.
Trav1
Trav11
Trav19
% of Trav1+
% of Trav11+
% of Trav19+
Proximal
Traj segments
Distal
e.
WT
Tcrd-/-
% of Traj18+
% of Traj33+
% of Traj57+
Trav-dv segments

approach and analyzed TCRα transcripts from CD4$^+$CD8$^+$-TCRβ$^{neg/int}$ DP thymocytes isolated as above. As *Tcrd*$^{-/-}$ mice were originally generated using 129 strain-derived embryonic stem cell lines before backcrossing to the C57BL/6 background, we aligned *Trav* gene segment sequences from our dataset to allelic reference sequences derived from various mouse strains (Supplementary Fig. 6B, IMGT,[40–42]). As a candidate proximal *Trav* gene segment, we aligned *Trav19* sequences obtained from WT and *Tcrd*$^{-/-}$ thymocytes to functional reference *Trav19* alleles, i.e., *Trav19*01* and *Trav19*03*. Based on single nucleotide polymorphisms (SNPs), WT and *Tcrd*$^{-/-}$ derived sequences differentially aligned to the *Trav19*03* and *Trav19*01* alleles, respectively (Supplementary Fig. 6B). Notably, *Trav19*03* and *Trav19*01* are derived from the C57BL/6J and 129/SvJ mouse strains, respectively[42]. The same was true for candidate distal *Trav1* and *Trav6-1* gene segments. *Tcrd*$^{-/-}$ *Trav1* and *Trav6-1* sequences aligned with the *Trav1*01* and *Trav6-1*01* alleles (129/SvJ strain), respectively, in contrast to C57BL/6 WT controls which aligned to *Trav1*02* and *Trav6-1*02* (C57BL/6J strain) (Supplementary Fig. 6B). These data suggest that *Trav* gene segments within the *Tcra-Tcrd* locus of *Tcrd*$^{-/-}$ mice are derived from 129-strain mice, reflecting the use of 129-strain embryonic stem cells to generate these mice[39]. Accordingly, analysis of DP thymocytes from 129T2/Sv mice revealed higher expression of *Trav1-Traj33* transcripts, that matched the levels of those from *Tcrd*$^{-/-}$ mice, relative to C57BL/6 WT mice but lower levels of *Trav11-Traj18* transcripts relative to both C57BL/6 WT and *Tcrd*$^{-/-}$ mice (Fig. 4B).

In addition to allelic variation, the structure of the *Tcra-Tcrd* locus itself varies between mouse strains[40,41]. C57BL/6, BALB/c, and 129 mice all harbor a duplication of a region of *Trav* gene segments (denoted 'd' e.g., *Trav7d-4*). However, C57BL/6 mice uniquely exhibit an additional duplication of *Trav* gene segments (denoted 'n' e.g., *Trav7n-4*) found in the center of the array of *Trav/Trdv* gene segments. This is referred to as the 'central repeat' region[40,41] (Supplementary Figs. 6A, B). Accordingly, alignments to central repeat *Trav* gene segments were much more frequent within C57BL/6-derived transcripts (~27% of total) relative to *Tcrd*$^{-/-}$-derived transcripts (~5.4%) (Fig. 4C), suggesting that *Tcrd*$^{-/-}$ mice lack the central repeat *Trav* gene segment region that is characteristic of C57BL/6 mice. Though some *Tcrd*$^{-/-}$ sequences aligned to central repeat gene segments, this was most likely explained by alignment to *Trav14n-1*. However, as *Trav14n-1* and *Trav14d-1* have virtually identical sequences, these alignments likely reflect high sequence homology between *Trav14n-1* and *Trav14d-1* rather than true alignments to central repeat gene segments (Supplementary Fig. 6B).

To gain a broader view of the TCRα repertoire within CD4$^+$-CD8$^+$TCRβ$^{neg/int}$ DP thymocytes, we analyzed the frequency of all *Trav* to *Traj* gene segment pairings within our dataset (Figs. 4C–E, Supplementary Fig. 6C). Consistent with previous reports, the rearrangement of *Trav* to *Traj* gene segments within C57BL/6 WT thymocytes also appeared to be processive and coordinated (Supplementary Fig. 6C)[40,43]. We additionally showed that the TCRα repertoire of thymocytes from C57BL/6 Vav-Bcl2 transgenic (Bcl2Tg) mice[44,45], in which Bcl2-overexpression in DP thymocytes leads to an increased DP thymocyte life span, was highly skewed toward rearrangements utilizing distal *Traj* gene segments (Supplementary Fig. 6C), in line with increased secondary TCRα rearrangements in these mice[44,45].

In *Tcrd*$^{-/-}$ thymocytes, the overall TCRα repertoire lacked pairings to central repeat *Trav* gene segments despite these pairings being present within C57BL/6 thymocytes (Figs. 4C–E, Supplementary Fig. 6C). Outside of the central repeat region, distal unique and proximal repeat *Trav* gene segment usage was increased in *Tcrd*$^{-/-}$ thymocytes relative to WT thymocytes (8.3% vs 5.4%, and 40.5% vs 23.2%, respectively) (Fig. 4C, Supplementary Fig. 6C). We quantified pairing of candidate distal (e.g. *Trav1*), central (e.g. *Trav11*), and proximal (e.g. *Trav19*) *Trav* gene segments and candidate *Traj* gene segments (*Traj18*, *Traj33*, and *Traj57*) to *Traj* and *Trav* segments, respectively (Figs. 4D and 4E). Approximately 1.8% and 2.3% of *Trav1*$^+$ transcripts from C57BL/6 and *Tcrd*$^{-/-}$ thymocytes, respectively, paired with *Traj33*, whereas 2.6% and 4.8% of *Traj33*$^+$ transcripts paired with *Trav1* (Figs. 4D and 4E), in line with an increase in the pairing of *Traj33* to distal unique gene segments overall (Fig. 4E). However, upon analysis of total *Traj18*$^+$ transcripts, though there was a decrease in pairings to *Trav11*, there was a concomitant increase in pairing to *Trav11d* in *Tcrd*$^{-/-}$ thymocytes relative to WT thymocytes. The lack of discrimination between *Trav11* and *Trav11d* potentially explains an overall similar level of the *Trav11-Traj18*$^+$ NKT-TCRα chain measured via qPCR (Fig. 4A). Accordingly, our data strongly suggest that *Tcrd*$^{-/-}$ mice harbor the *Tcra-Tcrd* locus derived from the 129-strain embryonic stem cells used to generate these mice, despite backcrossing to the C57BL/6

Fig. 4 Increased TCRα rearrangement in *Tcrd*$^{-/-}$ thymocytes facilitates increased generation of MAIT cells. (A) Graphs show the relative expression of *Trav1-Traj33*, *Trav11-Traj18*, and *Trac* transcripts (left) and *Trav1-Traj33* and *Trav11-Traj18* expression levels standardized to the levels of *Trac* expression (right) in thymocytes from indicated mouse strains analyzed by quantitative polymerase chain reaction. (B) Graphs show *Trav1-Traj33* and *Trav11-Traj18* expression levels standardized to the levels of *Trac* expression in thymocytes from C57BL/6 WT, *Tcrd*$^{-/-}$, and 129T2 WT mice (right) analyzed by quantitative polymerase chain reaction as in (A). (A & B) Relative expression was calculated as a fold change from the mean expression level (defined as 1) in WT mice (dotted line). Horizontal bars represent mean ± standard error of the mean. Each symbol represents an individual mouse. A total of 5–6 mice were examined across two independent experiments. * $p \leq 0.05$, ** $p \leq 0.01$ using a Mann-Whitney U test with a Bonferroni correction for three hypotheses. (C) Overall *Trav* gene segment usage as a percentage of total TCRα transcripts within thymocytes from C57BL/6 and *Tcrd*$^{-/-}$ mice. Data points depict mean ± SD, with a total of three mice per group across two independent experiments. Numbers above graphs represent collective percentage of *Trav* gene segment usage within indicated *Trav-dv* regions. (D & E) Graphs depict the frequency of pairings of indicated *Trav* (D) and *Traj* (E) gene segments to *Traj* and *Trav* segments as a percentage of all transcripts containing the indicated *Trav* or *Traj* gene segment in C57BL/6 and *Tcrd*$^{-/-}$ mouse thymocytes. Bar graphs depict mean ± SD with a total of three mice in each group, across two independent experiments. (E) Numbers above graphs represent collective percentage of *Trav* gene segment usage within indicated *Trav-dv* regions as in (C). MAIT = mucosal-associated invariant T cell; TCR = T cell receptor; WT = wild-type.

background. Moreover, this has resulted in an increase in TCRα chain rearrangements involving distal unique and proximal repeat *Trav* gene segments, such as *Trav1*, within *Tcrd*$^{-/-}$ mice relative to C57BL/6 WT controls (Fig. 4B–E). Consequently, the increased rearrangement of *Traj33* to *Trav1*, resulting in increased *Trav1-Traj33*$^{+}$ transcripts within developing *Tcrd*$^{-/-}$ thymocytes, may facilitate an increase in MAIT cell generation within and output from the *Tcrd*$^{-/-}$ thymus.

MAIT cells exhibit higher proliferative capacity in *Cd1d*$^{-/-}$*Tcrd*$^{-/-}$ mice

Despite increases in *Trav1-Traj33* rearrangement (Fig. 4) and MAIT cell levels in the thymus of *Tcrd*$^{-/-}$ mice relative to WT mice (Fig. 2), increases in MAIT cell levels in the periphery of both *Tcrd*$^{-/-}$ and *Cd1d*$^{-/-}$*Tcrd*$^{-/-}$ mice generally exceeded the increase observed in thymus, implying further expansion of MAIT cells in the periphery of mice lacking both NKT and γδT cells. Accordingly, we quantified homeostatic proliferation by MAIT cells by adoptive transfer of these cells into WT or *Cd1d*$^{-/-}$*Tcrd*$^{-/-}$ recipients. To circumvent the rarity of MAIT cells sourced from WT mice and to avoid TCR engagement by MR1-5-OP-RU-tetramers, we enriched for MAIT and other CD62L^{lo} T cell subsets by depleting B220- and CD62L-expressing cells from spleen and peripheral LNs (pLNs) of WT congenic Ly5.1 mouse donors prior to labeling with the proliferation dye, Cell Trace Violet (CTV), which resulted in an approximately 11-fold enrichment in MAIT cells (Fig. 5A), as well as enriching for NKT and CD44^{hi} γδT cells.

Eight days post-adoptive transfer, donor MAIT cells were recovered from the liver, spleen, and pLNsof recipient WT and *Cd1d*$^{-/-}$*Tcrd*$^{-/-}$ mice. However, donor MAIT cells were neither detected in, nor recovered from, the thymii of recipient mice (data not shown). Notably, donor MAIT cells recovered from *Cd1d*$^{-/-}$*Tcrd*$^{-/-}$ mice had higher levels of CTV dilution than those recovered from WT mice (Fig. 5B). This was exemplified in the division index (DI), both raw and normalized to WT (relative DI), of donor MAIT cells recovered from the liver, spleen, and pLNs of *Cd1d*$^{-/-}$*Tcrd*$^{-/-}$ mice being significantly higher than that of MAIT cells recovered from WT mice (Figs. 5B and 5C, Supplementary Fig. 7B). On average, the relative DIs of MAIT cells transferred into *Cd1d*$^{-/-}$*Tcrd*$^{-/-}$ mice were 3.5, 2.5, and 2.4 in the liver, spleen, and pLNs, respectively, implying that MAIT cells within *Cd1d*$^{-/-}$*Tcrd*$^{-/-}$ tissues undergo more divisions than those within WT tissues at the resting state (Figs. 5B and 5C). Similarly, a greater proportion of MAIT cells that have undergone at least one division (percent divided) were found in *Cd1d*$^{-/-}$*Tcrd*$^{-/-}$ tissues compared to WT tissues (Supplementary Figs. 7A, B), particularly in the liver and spleen. Aligning with a report by Matsuda *et al.*[46], NKT cells can survive and proliferate in the absence of CD1d which we confirm using our *Cd1d*$^{-/-}$*Tcrd*$^{-/-}$ mouse model. We report a similar observation with MAIT cells, where proliferating donor MAIT cells were recovered from *Mr1*$^{-/-}$ mice, indicating that MR1 is not necessary for the homeostatic survival of MAIT cells (Supplementary Fig. 7A). Interestingly, donor NKT cells recovered from the liver and spleen, and γδT cells recovered from the liver, spleen, and pLNs of recipient *Cd1d*$^{-/-}$*Tcrd*$^{-/-}$ mice, had significantly higher DIs relative to those recovered from WT organs, where increases in percent divided also reached significance (Supplementary Figs. 7B, C). In addition, we observed increases in the proliferation of donor non-MAIT/NKT/γδT αβT cells from *Cd1d*$^{-/-}$*Tcrd*$^{-/-}$ mice (Fig. 5C, Supplementary Fig. 7B, C). The relative DI of CD4^{+}CD8^{-} SP and CD4^{-}CD8^{+} SP αβT cells were only significantly increased within the liver, while that of CD4^{-}CD8^{-} DN αβT cells was significantly increased in both the spleen and liver. However, the relative DI of non-MAIT/NKT/γδT αβT cells was on average lower than that of MAIT cells examined within the same organ.

We additionally compared the phenotype of donor MAIT cells recovered from spleen, liver, and pLNs post-adoptive transfer to that of donor MAIT cells pre-transfer, and to that of endogenous MAIT cells within WT and *Cd1d*$^{-/-}$*Tcrd*$^{-/-}$ recipients. Prior to transfer, ~60% of donor MAIT cells were CD4^{-}CD8^{-} DN, with the CD4^{+}CD8^{-} and CD4^{-}CD8^{+} SP subsets representing less than 20% of MAIT cells (Figs. 5D and 5E). As previously reported, the expression of CD4 and CD8[36], (Supplementary Fig. 4A), and CD138[17], (Supplementary Fig. 4B) by MAIT cells varies between tissues. Notably, upon recovery of donor MAIT cells from specific recipient mouse organs, the phenotypic distribution of donor MAIT cells was similar to that of endogenous MAIT cells from the same organ. This was exemplified in the pLNs, where the CD4/CD8 co-receptor distribution of donor MAIT cells was heavily skewed toward the CD4^{+}CD8^{-} SP subset, with a concomitant decrease in CD4^{-}CD8^{+} SP and CD4^{-}CD8^{-} DN subsets rel-

Fig. 5 MAIT cells exhibit higher proliferative capacity in *Cd1d*$^{-/-}$*Tcrd*$^{-/-}$ mice. (A) Flow cytometry analysis of pooled inguinal, axillary, brachial, and cervical lymph nodes, and spleens from Ly5.1 mice pre- and post-enrichment via magnetic bead-depletion of B220- and CD62L-expressing cells (top). Cells were labeled with CTV after enrichment. Plots show B220^{-} lymphocytes and numbers in plots represent percentages. The percentage of MAIT cells pre- and post-enrichment out of total lymphocytes was graphed (bottom). Each symbol represents one independent experiment where 19–21 mice were pooled with a total of three independent experiments. (B) Flow cytometry analysis of CD45.1^{+} donor T cells isolated from liver, spleen, and pooled inguinal, axillary, and brachial pLNs of WT (left column) and *Cd1d*$^{-/-}$*Tcrd*$^{-/-}$ (right column) mice. Rectangle gates in plots are representative of CTV dilution gating strategy on MR1-5-OP-RU tetramer^{+} MAIT cells. Plots were generated by concatenation of two mice within the same group from the same experiment (C). The relative DI of MAIT, NKT, γδT, and the CD4/CD8 subsets of non-MAIT/NKT αβ T cells was graphed as a fold change from the average DI of cells from WT mice. Horizontal bars represent mean ± standard error of the mean. Each symbol represents an individual mouse, with a total of six mice per group across three independent experiments. $p > 0.05$ (not shown), * $p \leq 0.05$, ** $p \leq 0.01$ using a Mann-Whitney U test. (D) Flow cytometry analysis of CD4 and CD8 expression (top panel) and CD138 expression versus CD45.1 (bottom panel) of donor MAIT cells pre-adoptive transfer, and donor CD45.1^{+} (top) and non-donor/endogenous (bottom) MAIT cells recovered from indicated WT recipient tissues 8 days later. Number in plots show percentage of gated subpopulations within MAIT cells. (E) Proportions of CD4/8 and CD138$^{+/-}$ MAIT cell subsets [as in (D)] were graphed. Horizontal lines represent mean ± standard error of the mean. Each purple triangle represents one independent experiment, where 19–21 mice were pooled, where a total of three independent experiments were carried out. All other symbols represent an individual mouse for a total of six mice per group across three independent experiments. ab =; CD = clusters of differentiation; CTV = Cell Trace Violet; γδT = gamma-delta T; MAIT = mucosal-associated invariant T cell; NKT = natural killer T cells; pLN = peripheral lymph node; TCR = T cell receptor; WT = wild-type.

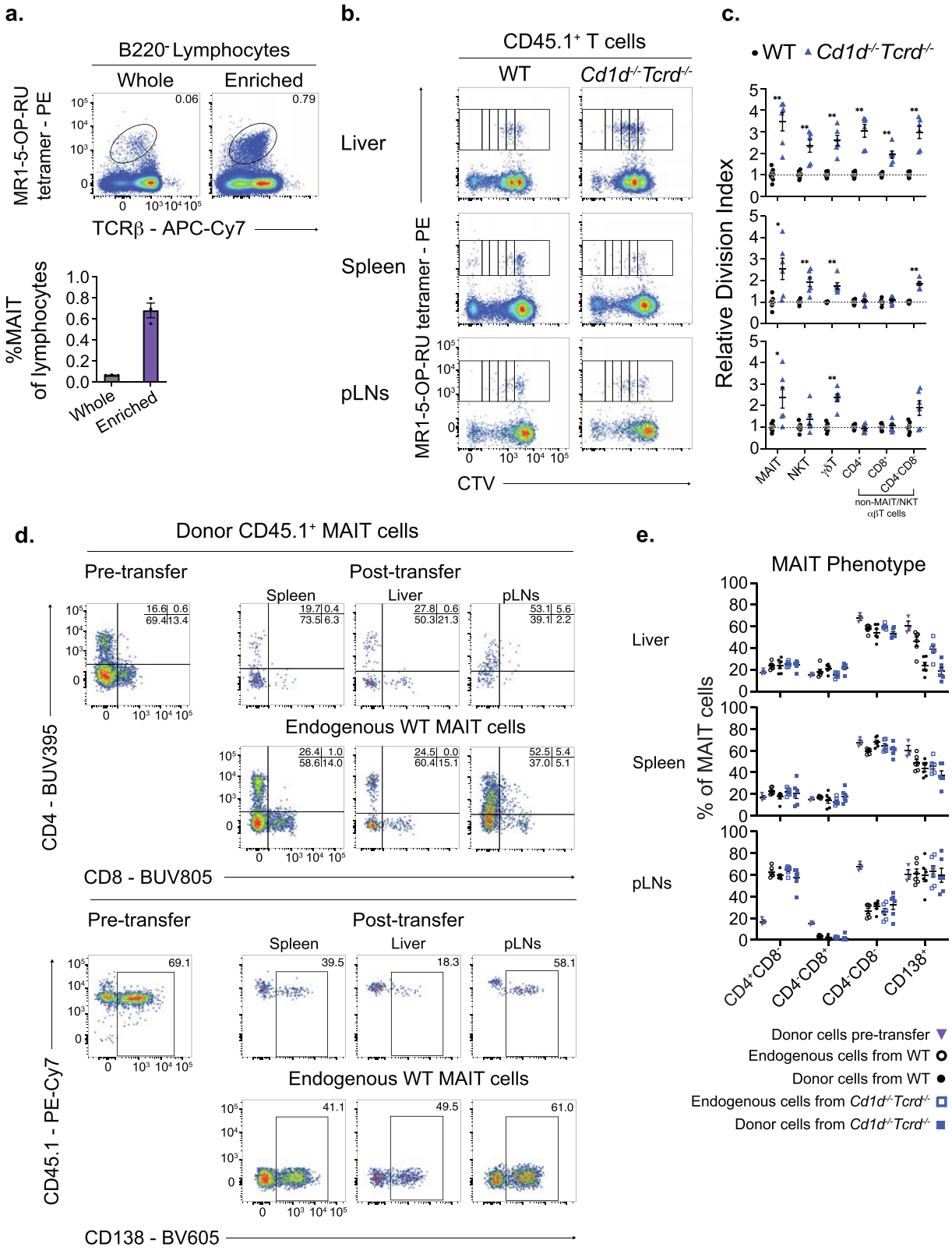
a.
B220⁻ Lymphocytes
Whole
Enriched
MR1-5-OP-RU tetramer - PE
0.06
0.79
TCRβ - APC-Cy7
%MAIT of lymphocytes
Whole
Enriched
b.
CD45.1⁺ T cells
WT
Cd1d-/-Tcrd-/-
Liver
Spleen
pLNs
MR1-5-OP-RU tetramer - PE
CTV
c.
WT
Cd1d-/-Tcrd-/-
Relative Division Index
MAIT
NKT
γδT
CD4⁺
CD8⁺
CD4⁻CD8⁻
non-MAIT/NKT αβT cells
d.
Donor CD45.1⁺ MAIT cells
Pre-transfer
Post-transfer
Spleen
Liver
pLNs
Endogenous WT MAIT cells
CD4 - BUV395
CD8 - BUV805
CD45.1 - PE-Cy7
CD138 - BV605
e.
MAIT Phenotype
Liver
Spleen
pLNs
% of MAIT cells
CD4⁺CD8⁻
CD4⁻CD8⁺
CD4⁻CD8⁻
CD138⁺
Donor cells pre-transfer
Endogenous cells from WT
Donor cells from WT
Endogenous cells from Cd1d-/-Tcrd-/-
Donor cells from Cd1d-/-Tcrd-/-

ative to pre-transfer MAIT cells (Fig. 5D). In addition, we observed a slight enrichment for donor CD4$^+$CD8$^-$ and CD4$^-$CD8$^+$ SP and a slight decrease in CD4$^-$CD8$^-$ DN MAIT cells in the liver of recipient mice relative to MAIT cells pre-transfer (Fig. 5D). Furthermore, donor MAIT cells recovered from pLNs were also predominantly CD138$^+$, matching that of donor cells pre-transfer and recipient endogenous pLN MAIT cells (Figs. 5D and 5E). In the spleen, a lower proportion (~40%) of donor MAIT cells were CD138$^+$ relative to cells pre-transfer (~60%), aligning with a similar proportion of endogenous CD138$^+$ MAIT cells. Interestingly, the frequency of CD138$^+$ donor MAIT cells recovered from the liver was lower than that of cells both pre-transfer (~60%) and endogenous MAIT cells (~40-50%).

Lastly, we found that donor NKT and γδT cells recovered from recipient mice also had a similar phenotype to endogenous NKT and γδT cells from the same tissue, as exemplified in pLNs and, to a lesser extent, liver (Supplementary Fig. 7D). For example, despite the vast majority (~93%) of donor γδT cells being CD4$^-$CD8$^-$ DN, only ~50% of donor γδT cells recovered from the pLNs were CD4$^-$CD8$^-$ DN, in line with that of endogenous pLN γδT cells and corresponding to a concomitant increase in recovered CD4$^+$ cells (Supplementary Fig. 7D). As donor cells were sourced from a mixture of spleen and pLN cells, it is possible that these findings result from redistribution and homing of adoptively transferred pLN donor cells back to the LNs over other tissues. However, it is also possible that splenic donor cells that enter pLNs respond to the LN microenvironment and upregulate characteristics of endogenous LN cells, such as high CD4 or CD138 expression on MAIT cells. Collectively, these data indicate that MAIT cells compete with NKT and γδT cells in the periphery within a common homeostatic niche and exhibit increased proliferation likely in response to tissue-specific microenvironmental signals in the absence of NKT and γδT cells.

Discussion

In this study, we provide evidence for a homeostatic niche shared by the unconventional T cell lineages, MAIT, NKT, and γδT cells. Though MAIT cells were increased in *Cd1d*$^{-/-}$ mice, suggesting that NKT and MAIT cells compete for similar factors, it was unknown whether this was due to the absence of competing type I and II NKT cells, or through an NKT cell-independent role for *Cd1d* in regulating MAIT cell numbers. Although MAIT cells were expanded in *Traj18*$^{-/-}$ mice, which retain type II NKT cells and *Cd1d*, they were further expanded in *Cd1d*$^{-/-}$ mice which lack both type I and type II NKT cells. Notwithstanding the overall observation, there remained some overlap in the frequency of MAIT cells between several *Traj18*$^{-/-}$and *Cd1d*$^{-/-}$ mice when compared to WT mice. MAIT cells are known to vary in frequency in mice and humans[36,47], which may explain this partial overlap and suggests that there are other, as yet unknown, variables driving this phenotype. MAIT cells were also expanded in *Tcrd*$^{-/-}$ mice[23,27,28], and the most striking observation came from *Cd1d*$^{-/-}$*Tcrd*$^{-/-}$ mice, where the absence of both NKT cells and γδT cells resulted in a large increase in MAIT cells. As γδT and NKT cells within *Cd1d*$^{-/-}$ and *Tcrd*$^{-/-}$ mice, respectively, outnumber MAIT cells within the same tissue sites, these two cell types may outcompete MAIT cells for shared factors, explaining the greater expansion of MAIT cells in the absence of both NKT and γδT cells. Though it is tempting to speculate that redundancies exist within the unconventional T cell compartment and that MAIT cells compensate for a loss of NKT and γδT cells, this compensation is only partial, as MAIT cell numbers in *Cd1d*$^{-/-}$*Tcrd*$^{-/-}$ mice do not reach NKT and γδT cell levels seen in WT mice, and furthermore, these cell types have distinct antigenic targets so their function is unlikely to be redundant.

While our study focused on unconventional T cells, and found that non-MAIT/NKT CD4$^-$CD8$^-$ DN αβT cells and PLZF$^+$ αβT cells do not appear to be increased in *Cd1d*$^{-/-}$*Tcrd*$^{-/-}$ mice, further studies should investigate whether other cells (T and non-T cells) are also competing within this niche. Indeed, a population of MHC-independent αβ dendritic epidermal T cells has been described to compensate for the absence of skin-resident γδT cells in *Tcrd*$^{-/-}$ mice[48]. Though we have demonstrated increases in MAIT cells in our mouse models at steady state, it will be interesting to determine the extent to which these expanded MAIT cells can compensate for the loss of NKT and γδT cell-mediated immune responses. Indeed, the concept of unconventional T cells acting in concert as a functional unit has been recently explored in type-1 and type-17 responses within the lymph nodes[49].

We further showed elevated homeostatic proliferation of MAIT cells in the periphery of *Cd1d*$^{-/-}$*Tcrd*$^{-/-}$ mice, supporting the existence of a competitive niche between MAIT cells and other unconventional T cells. Homeostatic cytokines likely represent factors for which unconventional T-cell populations compete, as supported by existing reports and high expression of cytokine receptors on unconventional T cells. For example, IL-7R is highly expressed on NKT-17[30], γδT-17[31], and MAIT-17[17] cells, also shown in our data. In line with this, IL-7 is required for the survival and homeostasis of NKT-17[30] and γδT-17 cells[31,50,51], and *in vivo* administration of IL-7 leads to the expansion of NKT-17, γδT-17, and MAIT-17 cells in the lungs[34]. In addition, NKT-17, γδT-17, and MAIT-17 cells also are responsive to IL-1β and/or IL-23[33,52,53]. In contrast, T-bet$^+$ unconventional T cells express high levels of IL-2R, where IL-2 and IL-15 appear to expand or regulate the homeostasis of NKT-1, γδT-1, and MAIT-1 cells[30–33]. Furthermore, the presentation of IL-15 by thymic epithelial cells or peripheral sources influences the development of T-bet$^+$ 'type 1 innate T cells'[54–56]. Given that unconventional T cells of similar functions share common differentiation and transcriptomic programs, it is reasonable to hypothesize that they respond to similar cues during development, maturation, and functional polarization. However, here we observed a global expansion of both MAIT-1 and MAIT-17 cells, suggesting that this is driven by reduced competition for a factor that governs both cell types, or a combination of factors that may include IL-7 and IL-15. Although analysis of whole tissue *Il-7* and *Il-15* transcripts revealed no difference in WT and *Cd1d*$^{-/-}$*Tcrd*$^{-/-}$ mouse tissues, cellular subsets within the competitive niche are likely shaped by distinct contexts and/or tissue sites. For example, increased proliferation of non-MAIT/NKT αβT cells was most prominent in the liver, likely reflecting the loss of both NKT and γδT cells which collectively make up to 50% of T cells in this organ[57].

A limitation of this study is that we have not investigated potential relationships between microbiota composition and MAIT cell numbers within our mouse models. Unconventional T cells often represent a sizable portion of cells in mucosal and barrier tissues such as the gut and lungs, where they may interact with microbiota[36,58,59]. Indeed, deficiencies in NKT and/or γδT cells have been linked to altered microbiota composition, however, these studies lacked specific littermate-controlled experiments to allow definite conclusions, as recently discussed[60]. The influence of microbiota on unconventional

T-cell populations is an important area of investigation, including studies suggesting that the liver hosts distinct microbiota that can modulate NKT cells[61], and metabolites of microbial origin can traffic from the gut to other organs, including the thymus, to modulate MAIT cell development[62,63]. Thus, increased microbial burden (within NKT and/or γδT cell-deficient mice) and subsequent translocation of microbial products across barrier tissues to which MAIT cells can respond, may lead to an increase in peripheral or organ-specific MAIT cell levels, or affect the composition of the unconventional T-cell niche.

Our study also provides evidence for an additional mechanism that may influence MAIT cell numbers in *Tcrd*$^{-/-}$ mice, where increased distal *Trav* gene segment rearrangement led to an increase in *Trav1-Traj33* usage within *Tcrd*$^{-/-}$ thymocytes due to strain-associated *Tcra-Tcrd* locus genetics. Several reports have previously linked TCRα chain rearrangement dynamics to MAIT cell development and frequency. In generating *Traj18*$^{-/-}$ mice, the genetic deletion of *Traj18* via PGK-neo^{r} cassette insertion inadvertently disrupted TCR rearrangements using genes encoding *Traj* gene segments upstream of *Traj18*, including *Traj33*[35]. Thus, these *Traj18*$^{-/-}$ mice were deficient in *Trav1-Traj33*$^{+}$ MAIT cells[64,65]. In addition, relative to the C57BL/6 and BALB/c strains, the elevated MAIT cell numbers in the CAST/EiJ mouse strain were linked to increased MAIT-TCRα rearrangements and overall increased usage of distal *Trav* gene segments, including *Trav1* itself, a phenotype mapped to a single 20 Mb region within the *Tcra-Tcrd* locus[41]. It is known that rearrangement of *Tcrd* gene segments, i.e. *Trdv*, *Trdd*, and *Trdj*, to *Trdc* within DN thymocytes, variably truncates the *Tcra-Tcrd* locus and increases accessibility of distal *Trav* gene segments, such as *Trav1*, in pairing with more proximally and centrally-located *Traj* segments, such as *Traj33*, in primary TCRα chain gene rearrangements[43]. In line with this, modifications of the TCR locus perturbs *Tcrd* rearrangement in TCR transgenic (HYα) and INT1 and INT2 CCCTC-binding factor site-deleted (INT1-2-deficient) mouse models, respectively, resulting in reduced *Trav1-Traj33* rearrangements in the thymus and lower MAIT cell numbers in the periphery of these mice[43]. Here, our findings indicate that the *Tcra-Tcrd* locus within *Tcrd*$^{-/-}$ mice has been retained from the original 129-derived embryonic stem cell strain used for their generation, despite 12 backcrosses to the C57BL/6 background[39]. The increase in *Traj* to distal *Trav* pairing likely accounts for increased *Trav1-Traj33* rearrangements within *Tcrd*$^{-/-}$ thymocytes relative to C57BL/6 thymocytes. This in turn may contribute to the elevated generation of MAIT cells in the *Tcrd*$^{-/-}$ thymus. However, as BALB/c mice also lack central repeat *Trav* gene segments yet have fewer thymic MAIT cells compared to C57BL/6 mice, differences in *Trav* rearrangements may not fully explain the variability of MAIT cell numbers within distinct mouse strains. Nevertheless, our study reinforces the unique relationship between TCRα rearrangement kinetics and MAIT cell development, which for example, may impact the interpretation of studies using *Tcrd*$^{-/-}$ mice[39] as a means to understand the role of γδT cells, because these mice not only lack γδT cells, but also have increased MAIT cells. This illustrates the need for the generation of γδT cell-deficient mice using CRISPR-mediated excision of *Trdc* or *Trgc* on the strain background of choice for accurate comparisons between γδT cell-deficient mice with WT controls.

Despite advances in the identification and characterization of mouse MAIT cells[36,66], the paucity of MAIT cells in most laboratory mouse strains can impede the isolation of MAIT cells. Importantly, *Cd1d*$^{-/-}$*Tcrd*$^{-/-}$ mouse MAIT cells exhibit a similar phenotype and function to WT MAIT cells, thus these mice could be used as a source of these cells for studying the role of MAIT cells in disease models. Furthermore, regardless of the strain we examined, our analysis revealed a mouse hepatic RORγt^{+}T-bet^{+} MAIT cell subset that resembles *Salmonella*- or *Legionella*-expanded murine lung MAIT cells[67,68], IL-1β and IL-23-treated murine MAIT cells[33], and steady-state human MAIT cells[47,69,70]. However, we did not see a population of IL-17A^{+} cells that could also produce IFN-γ, contrasting the predominant IFN-γ production from circulatory or non-IL-7-licensed human RORγt^{+}T-bet^{+} MAIT cells[71,72]. We also highlight the use of CD319 as a pan T-bet^{+} unconventional T cell-surface surrogate marker, in addition to previously described candidates such as CD122, NK1.1, and CXCR3[16,17,73].

In contrast to mice, the composition of the human unconventional T cell compartment is marked by a relative abundance of MAIT and γδT cells, and paucity of NKT cells[1,47], where an interplay between these cell types at homeostasis has been suggested. Despite frequencies of MAIT, NKT, and γδT cells widely varying between individuals, the frequencies of circulating MAIT and Vδ2^{+} γδT cells, and of MAIT and NKT cells within healthy human donors have been shown to positively correlate[47,74]. Thus, it is tempting to speculate that human unconventional T cells may also respond to an increased abundance of common growth or survival factors within the circulation or within tissues. Notably, a case study on an individual that had both a point mutation in MR1 and a lack of circulating MAIT cells, possessed a marked expansion of Vδ2^{+} γδT cells[75]. These studies, in addition to our own findings, strongly suggest an intertwined system for complementary functions and redundancy within the unconventional T-cell compartment[76].

In conclusion, we emphasize an interplay between unconventional T-cell populations at the steady state. As MAIT, NKT, and γδT cells are attractive cellular targets that can bypass donor-to-donor restrictions and differences in genetic background[77], this study highlights the importance of considering all subsets of unconventional T cells as complementary or confounding factors when targeted in immunotherapeutic applications. Finally, we highlight the fact that mouse models that lack NKT cells, γδT cells, or both, have a compensatory increase in MAIT cells. While this sheds light on how the numbers of these cells may be regulated, this also represents a variable that may complicate interpretation of data from studies using these mice.

METHODS

Mouse models

Colonies on a BALB/c background used were BALB/c wild-type (WT), BALB/c *Traj18*-deficient (generated by Cas9-mediated introduction of a null mutation into *Traj18*[78]) and BALB/c *Cd1d*$^{-/-}$ (*Cd1d1.Cd1d2*-deficient, 11 backcrosses[79]). C57BL/6 colonies used were C57BL/6 wild-type (B6 WT), C57BL/6 Ly5.1 wild-type, *Cd1d*$^{-/-}$ (11 backcrosses[80]; originally obtained from Jackson Laboratories), *Tcrd*$^{-/-}$, (12 backcrosses[39]; originally obtained from Jackson Laboratories), *Cd1d*$^{-/-}$*Mr1*$^{-/-}$ and *Cd1d*$^{-/-}$*Tcrd*$^{-/-}$ double knockout mice. *Cd1d*$^{-/-}$*Tcrd*$^{-/-}$ mice were generated in-house by breeding *Cd1d*$^{-/-}$ and *Tcrd*$^{-/-}$ mice to create heterozygous F_1 mice, which were then mated to generate homozygous *Cd1d*$^{-/-}$*Tcrd*$^{-/-}$ mice, phenotyped with flow cytometry analysis to confirm the lack of γδTCR^{+} (clone GL3) and CD1d-α-GalCer (PBS-44, a kind gift from Dr. Paul Savage, Brigham Young University; Provo, UT) tetramer^{+} cells. *Cd1d*$^{-/-}$*Mr1*$^{-/-}$ mice were

generated in-house by breeding *Cd1d*$^{-/-}$ and *Mr1*$^{-/-}$ mice to create heterozygous F_1 mice, which were then mated to generate homozygous *Cd1d*$^{-/-}$*Mr1*$^{-/-}$ mice, phenotyped with flow cytometry analysis to confirm the lack of CD1d-α-GalCer tetramer$^+$ cells and MR1-5-OP-RU tetramer$^+$ cells. All mice were bred in-house at the Department of Microbiology and Immunology Animal House, University of Melbourne under specific pathogen-free conditions. C57BL/6 Ly5.1 mice were purchased from Animal Resource Centre (ARC, Western Australia). 129T2/Sv WT mice were purchased from the Kew Bioservices facility, Walter and Eliza Hall Institute of Medical Research. All male and female mice used in experiments were between 6-12 weeks old and were all age- and sex-matched. All procedures on mice were approved by the University of Melbourne Animal Ethics Committee (#1914739).

Preparation of cell suspensions

Single-cell suspensions of thymus, spleen, and lymph node tissues were prepared by carefully grinding each organ through a 30-μM nylon cell strainer into ice-cold FACS buffer (phosphate buffered saline (PBS) with 2% FCS). Spleen suspensions were also treated with red blood cell lysis buffer and subsequently washed with FACS buffer. Splenic enrichments were achieved by labeling B220^{high} splenocytes with magnetic beads and collecting unlabeled cells as per manufacturer's instructions (Miltenyi Biotec). Prior to organ harvest, the liver was perfused with PBS after culling mice. Liver tissue was then dissociated by grinding through a 70-μM nylon mesh filter into ice-cold FACS buffer. Hepatic leukocytes were then isolated using a Percoll gradient (GE Healthcare) before being treated with red blood cell lysis buffer and further washed with FACS buffer. Lungs were perfused with PBS prior to harvest and minced into a fine suspension before enzymatically digested in collagenase type III (Worthington Biochemical Corporation: 3 mg/ml in RMPI-1640 supplemented with 2% FCS and 5 μg/ml DNase I (Roche)) for 40 minutes at 37°C. After digestion, the cell suspension was filtered through a 30-μM nylon cell strainer and then treated with red blood cell lysis buffer for 5 minutes at room temperature before washing with FACS buffer. Mouse gut tissues were processed for IELs. IELs were isolated from the large intestine by first removing associated fat and Peyers patches. The large intestine was cut longitudinally to allow efficient removal of fecal and mucosal contents. Subsequent cuts were made to obtain ~1 cm^2 pieces, which were digested in Ca^{2+} and Mg^{2+} Free Hanks buffer containing 1 mM DTT and 10% FCS. IELs were released from the epithelial fraction by vigorous vortexing and passed through a 70-um strainer. IELs were resuspended in 44% Percoll and underlaid with 70% Percoll for density gradient centrifugation.

Tetramer production

Tetramers of mouse MR1-5-OP-RU were generated as previously reported[81] by refolding MR1 monomers in the presence of 5-A-RU and methylglyoxal. Mouse MR1-Ac-6-FP tetramers were also generated as previously described[82]. MR1-Ag monomers were then enzymatically biotinylated with BirA enzyme followed by purification by size exclusion chromatography. Biotinylated MR1-5-OP-RU and MR1-Ac-6-FP monomers were tetramerized using streptavidin conjugated to PE (SAv-PE; Invitrogen Molecular Probes).

Soluble mouse CD1d/β_2m protein was produced as previously described[83]. Purified CD1d-biotin was loaded with the α-GalCer analog, PBS-44, a gift of P. Savage (Brigham Young University, Provo, UT) at room temperature overnight at a 6:1 (lipid:protein) molar ratio. CD1d loaded with PBS-44 hereby referred to as CD1d-α-GalCer, or in the presence of the vehicle in which PBS-44 was solubilized (CD1d-vehicle), was tetramerized with streptavidin conjugated to Brilliant Violet 421 (SAv-BV421; BioLegend) or Alexa-Fluor647 (SAv-AF647; BioLegend). SAv-PE, SAv-BV421, or SAv-AF647 were added via four additions of one-quarter of the required volume with an incubation of 10 minutes in the dark at 4̊C, and mixing between additions.

Flow cytometry

Cell-surface staining

Cells were first stained with PE-conjugated MR1-5-OP-RU or MR1-Ac-6-FP tetramers alongside 7-aminoactinomycin D (7-AAD; Sigma-Aldrich), and the cell-surface antibodies as listed in Supplementary Table 1. For MR1 upregulation experiments, cells were incubated with or without 100nM Ac-6-FP overnight prior to labelling with anti-MR1 mAbs. For all flow cytometry experiments, cells were incubated at 4̊C in the dark for 30 minutes, before being washed and labeled with CD1d-α-GalCer or CD1d-vehicle tetramers conjugated to BV421, PE, or AF647 at 4̊C in the dark for 30 minutes. Cells were then analyzed using a BD LSR Fortessa equipped with a 561-nm yellow-green laser. Data were analyzed using FlowJo software (BD). After excluding dead cells and doublets by electronic gating, B220$^-$ lymphocytes were then gated on for further analysis.

Intracellular transcription factor staining

After surface staining, cells were fixed and permeabilized using the Foxp3 transcription factor staining kit (eBioscience) for 35 minutes at 4̊C in the dark. Cells were then washed and stained with anti-RORγt (APC; clone B2D; eBioscience, or BV786; clone Q31-378; BD), anti-T-bet (PE-Cy7; clone eBio4B10, eBioscience, or BV711; clone 4B10; BioLegend), and anti-PLZF (AF488; clone Mags.21F7; eBioscience, or PE-Cy7; clone 9E12; eBioscience).

Intracellular cytokine staining

Thymus, spleen, and liver cell suspensions were stimulated with PMA (10 ng/ml; Sigma-Aldrich) and ionomycin (1 μg/ml; Sigma-Aldrich) in the presence of both GolgiStop and GolgiPlug (BD Biosciences) and 10 μM of the P2X7 inhibitor, A438079 (Santa Cruz Biotechnology, sc-203788). After 4 hours of stimulation at 37̊C, cells were washed with FACS buffer and then underwent cell-surface staining. Prior to staining for intracellular cytokines, cells were then fixed and permeabilized using the BD Cytofix/Cytoperm kit (BD Biosciences) in accordance with the manufacturer's instructions. Cells were then stained for anti-IL-17A (AF647; clone TC11-18H10; BD Biosciences) and anti-IFN-γ (FITC; clone XMG12; BioLegend) for flow cytometric analysis.

RNA extraction and cDNA synthesis

3-4 x 10^6 CD4$^+$CD8$^+$ DP TCRβ$^{-/low}$ MR1-5-OP-RU-tetramer and CD1d-α-GalCer-tetramer negative thymocytes were bulk sorted into ice-cold FACS buffer. In some experiments, total RNA was extracted from 4-5 x 10^6 cells from single-cell suspensions of the thymus, spleen, iLNs, and liver processed as above. Total RNA was extracted from each sample using the ISOLATE II RNA Mini Kit (Bioline) as per manufacturer's instructions. RNA purity (260/280nm ratio) and concentration were measured using the NanoDrop spectrophotometer LITE (Thermo Fisher Scientific) in order to standardize the amount of input RNA for

reverse transcription into cDNA using the SuperScript VILO kit (Invitrogen).

Quantitative PCR

qPCR was performed on the QuantStudio7 Flex Real-Time PCR System (Thermo Fisher Scientific) in triplicate and using the Power SYBR Green Master Mix (Thermo Fisher Scientific). Relative expression (RE) was calculated as previously described[84]. Briefly, the RE of each target gene, i.e, MAIT-TCRα chain (*Trav1-Traj33*), NKT-TCRα chain (*Traj11-Traj18*), and *Trac* (*Trac*-5′-*Trac*-3′), was calculated in all cDNA samples relative to the average of WT samples and compared to the average of all reference genes (*Gapdh*, *Hprt*, *Ppid*, *Tubb*) for each sample. For *Il15* and *Il7* mRNA transcript analysis, RE was calculated in all cDNA samples using the 2^{-DDCq} method relative to the average of WT samples. Gene expression was standardised to the *Gapdh* and *Hprt* reference genes.

Oligonucleotides

The following mouse primers for qPCR were used as previously published[41,85,86,87,88]: *Trav1*, CTTTCCTGAGCCGCTCGAA; *Traj33*, CTTGGTCCCAGAGCCCC; *Trav11* TGGGAGATACTCAGCAACTCTGG; *Traj18*, CCAGCTCCAAAATGCAGCC; *Trac*-5′, CCTCTGCCTGTTCACCGACTT; *Trac*-3′, CGGTCAACGTGGCATCACA; Gapdh-5′, TGTCCGTCGTGGATCTGAC. Gapdh-3′, CCTGCTTCACCACCTTCTTG; *Hprt*-5′, TCCTCCTCAGACCGCTTTT; *Hprt*-3′, CCTGGTTCATCATCGCTAATC; *Ppid*-5′, ATGGTGAAAAACCTGCCAAA; *Ppid*-3′, CATCCTCAGGGAAGTCTGGA; *Tubb*-5′, GCGCATCAGCGTATACTACAA; *Tubb*-3′, TTCCAAGTCCACCAGAATGG; *Il15*-5′, GTGACTTTCATCCCAGTTGC; *Il15*-3′, TTCCTTGCAGCCAGATTCTG; *Il7*-5′, CTGATGATCAGCATCGATGAATTGG; *Il7*-3′, GCAGCACGATTTAGAAAAGCAGCTT.

TCR deep sequencing

RNA from 3-4 x 10^6 $CD4^+CD8^+$ DP $TCR\beta^{-/low}$ MR1-5-OP-RU-tetramer-negative and CD1d-α-GalCer-tetramer-negative thymocytes was extracted as described above. Preparation of cDNA libraries for TCRα chain sequencing was conducted using the SMARTer Mouse TCR a/b Profiling Kit (Takara Bio). Sequencing of cDNA libraries was performed using the 600-cycle MiSeq Reagent Kit v3 (Illumina) with paired-end, 2 x 300 base-pair reads.

TCR repertoire analysis

TCR deep sequencing data was analyzed using MiXCR (v.3.0.13) with the standard immune repertoire analysis pipeline whereby sequences were aligned to a reference library comprised of 129 and C57BL/6 Vα/δ (*Trav/Trdv*) sequences and DBA/J Jα (*Traj*) sequences and clones identified and exported using the same package. Representatives of each *Trav* sequence were sampled and manually aligned against the reference library to ensure alignment accuracy. Recombination frequencies were calculated using custom Python scripts with corresponding heatmap plots generated using seaborn[89] and bar plots generated with Prism software from GraphPad.

MAIT cell enrichment, adoptive transfer, and recovery

For enrichment of MAIT cells, cell suspensions of inguinal, axillary, brachial, and cervical lymph nodes, and spleens from WT Ly5.1 congenic mice were pooled before depletion of B220- and CD62L-expressing cells using a mixture of CD45R (B220) and CD62L microbeads in accordance with manufacturer guidelines (Miltenyi Biotec). Mice were injected intravenously with 50μg of the ARTC2.2 blocking nanobody (S+16a; T-reg Protector, BioLegend) diluted in 200μL of sterile PBS 30 min prior to sacrifice and organ harvesting as previously described[90]. The enriched fraction of cells was labeled with CTV in accordance with manufacturer's guidelines (Thermo Fisher Scientific). Labeled cells were resuspended into sterile PBS and intravenously injected into the tail veins of recipient mice. Recipient mice were culled 8 days later and the spleen, liver, thymus, and inguinal, axillary, and brachial LNs were analyzed by flow cytometry. To facilitate recovery of adoptively transferred MAIT cells, B220-expressing cells were depleted from recipient mouse spleens using B220 MicroBeads (Miltenyi Biotec), and recipient mouse livers were not perfused with PBS prior to harvest.

Calculation of division index and percent divided

The division index (DI) is defined as the average number of divisions a cell in the original population has undergone. This was calculated using the following equation:

$$DI = \frac{\sum_0^i i \times \left(\frac{N_i}{2^i}\right)}{\sum_0^i \frac{N_i}{2^i}}$$

where i is the generation peak number (0 is defined as the rightmost peak, the undivided population) and N_i is the number of cells in generation i.

The percent divided (%D) is defined as the percentage of cells in the original, undivided population that have undergone at least one division. This was calculated using the following equation:

$$\%D = \frac{\sum_1^i \frac{N_i}{2^i}}{\sum_0^i \frac{N_i}{2^i}}$$

where i is the generation peak number (0 is defined as the rightmost peak, the undivided population) and N_i is the number of cells in generation i. N_1 is the number of cells in generation 1, the first peak to the left of the rightmost (brightest) peak.

AUTHOR CONTRIBUTIONS

C.X. and H.F.K. designed and performed experiments, analyzed and interpreted results, and wrote the manuscript, with input from authors D.G.P. and D.I.G.. S.L. and T.S.F. analyzed and interpreted results, S.N.C. performed experiments. L.K.M., D.H.D.G., A.P.U. provided key reagents, mice, and intellectual input, and approved the manuscript. D.G.P., D.I.G., and H.F.K. conceived and led the study.

DECLARATIONS OF COMPETING INTEREST

D.I.G. and A.P.U. have provisional patent applications submitted regarding targeting of unconventional T cells and their ligands for immunotherapy, and new vaccine approaches for COVID-19. All other authors declare no competing interests.

FUNDING

This work was supported by the National Health and Medical Research Council of Australia (NHMRC; 1113293, 1140126, and 1145373) and the Australian Research Council (ARC; CE140100011). C.X. is supported by an Australian Postgraduate Award, L.K.M is a Senior Medical Research Fellow supported by the Sylvia and Charles Viertel Charitable Foundation, D.H.D.G. is supported by an NHMRC Senior Research Fellowship (1158024), D.G.P. is supported by a CSL Centenary Fellowship,

D.I.G. was supported by an NHMRC SPRF fellowship (1117766) and is now supported by an NHMRC Investigator grant (2008913), H.F.K. was supported by an NHMRC ECF fellowship (1160333) and is now supported by an ARC DECRA (DE220100830).

DATA AVAILABILITY

The authors declare that the data supporting the findings of this study are available within the article, supplementary information files, and source data, or are available upon reasonable requests to the authors. TCRseq data are deposited to Sequence Read Archive, at the National Library of Medicine, National Institutes of Health, with the accession PRJNA804689.

ACKNOWLEDGMENTS

The authors thank Dr Marco Herold and Dr Andrew Kueh from Walter and Eliza Hall Institute for generating and providing *Traj18* gene-deleted heterozygous mice, supported by Phenomics Australia and the Australian Government through the National Collaborative Research Infrastructure Strategy (NCRIS) program. We thank Prof. Mitchell Kronenberg, Dr. Mallory Paynich, Dr. Catherine Crosby, Dr. Nadine Hartmann, A/Prof. Michele Teng, and Dr. Lynette Beattie for helpful discussions. We thank the staff in the Doherty Institute Animal House for animal husbandry assistance. We also thank Tina Luke and staff at the Doherty Institute Flow Cytometry Facility, and Vanta Jameson and staff at the Melbourne Brain Centre Flow Cytometry Facility, for flow cytometry support. Sequencing services utilized in this report were provided by the Australian Genome Research Facility (AGRF).

APPENDIX A. SUPPLEMENTARY DATA

Supplementary data to this article can be found online at https://doi.org/10.1016/j.mucimm.2023.05.003.

REFERENCES

1. Godfrey, D. I., Uldrich, A. P., McCluskey, J., Rossjohn, J. & Moody, D. B. The burgeoning family of unconventional T cells. *Nat. Immunol.* **16**, 1114–1123 (2015).
2. Klenerman, P., Hinks, T. S. C. & Ussher, J. E. Biological functions of MAIT cells in tissues. *Mol. Immunol.* **130**, 154–158 (2021).
3. Godfrey, D. I., Koay, H. F., McCluskey, J. & Gherardin, N. A. The biology and functional importance of MAIT cells. *Nat. Immunol.* **20**, 1110–1128 (2019).
4. Yamamoto, R. et al. Thymic development of a unique bone marrow-resident innate-like T cell subset with a potent innate immune function. *J. Immunol.* **203**, 167–177 (2019).
5. Vivier, E. et al. Innate lymphoid cells: 10 years on. *Cell* **174**, 1054–1066 (2018).
6. Olivares-Villagómez, D. & Van Kaer, L. Intestinal intraepithelial lymphocytes: sentinels of the mucosal barrier. *Trends Immunol.* **39**, 264–275 (2018).
7. Ribot, J. C., Lopes, N. & Silva-Santos, B. γδ T cells in tissue physiology and surveillance. *Nat. Rev. Immunol.* **21**, 221–232 (2021).
8. Pellicci, D. G., Koay, H. F. & Berzins, S. P. Thymic development of unconventional T cells: how NKT cells, MAIT cells and γδ T cells emerge. *Nat. Rev. Immunol.* **20**, 756–770 (2020).
9. Ciofani, M. & Zúñiga-Pflücker, J. C. Determining γδ versus αß T cell development. *Nat. Rev. Immunol.* **10**, 657–663 (2010).
10. Godfrey, D. I. & Berzins, S. P. Control points in NKT-cell development. *Nat. Rev. Immunol.* **7**, 505–518 (2007).
11. Bendelac, A., Savage, P. B. & Teyton, L. The biology of NKT cells. *Annu. Rev. Immunol.* **25**, 297–336 (2007).
12. Koay, H. F., Godfrey, D. I. & Pellicci, D. G. Development of mucosal-associated invariant T cells. *Immunol. Cell Biol.* **96**, 598–606 (2018).
13. Seach, N. et al. Double-positive thymocytes select mucosal-associated invariant T cells. *J. Immunol.* **191**, 6002–6009 (2013).
14. Griewank, K. et al. Homotypic interactions mediated by Slamf1 and Slamf6 receptors control NKT cell lineage development. *Immunity* **27**, 751–762 (2007).
15. Chen, S. et al. Dissection of SAP-dependent and SAP-independent SLAM family signaling in NKT cell development and humoral immunity. *J. Exp. Med.* **214**, 475–489 (2017).
16. Legoux, F. et al. Molecular mechanisms of lineage decisions in metabolite-specific T cells. *Nat. Immunol.* **20**, 1244–1255 (2019).
17. Koay, H. F. et al. A divergent transcriptional landscape underpins the development and functional branching of MAIT cells. *Sci. Immunol.* **4**, eaay6039 (2019).
18. Savage, A. K. et al. The transcription factor PLZF directs the effector program of the NKT cell lineage. *Immunity* **29**, 391–403 (2008).
19. Koay, H. F. et al. A three-stage intrathymic development pathway for the mucosal-associated invariant T cell lineage. *Nat. Immunol.* **17**, 1300–1311 (2016).
20. Kreslavsky, T. et al. TCR-inducible PLZF transcription factor required for innate phenotype of a subset of gammadelta T cells with restricted TCR diversity. *Proc. Natl Acad. Sci. U. S. A.* **106**, 12453–12458 (2009).
21. Lu, Y., Cao, X., Zhang, X. & Kovalovsky, D. PLZF Controls the Development of Fetal-Derived IL-17+Vγ6+ γδ T cells. *J. Immunol.* **195**, 4273–4281 (2015).
22. Salou, M. et al. A common transcriptomic program acquired in the thymus defines tissue residency of MAIT and NKT subsets. *J. Exp. Med.* **216**, 133–151 (2019).
23. Lee, M. et al. Single-cell RNA sequencing identifies shared differentiation paths of mouse thymic innate T cells. *Nat. Commun.* **11**, 4367 (2020).
24. Harsha Krovi, S. et al. Thymic iNKT single cell analyses unmask the common developmental program of mouse innate T cells. *Nat. Commun.* **11**, 6238 (2020).
25. Lee, Y. J. et al. Lineage-Specific Effector Signatures of Invariant NKT Cells Are Shared amongst γδ T, Innate Lymphoid, and Th Cells. *J. Immunol.* **197**, 1460–1470 (2016).
26. Parker, M. E. & Ciofani, M. Regulation of γδ T cell Effector Diversification in the Thymus. *Front. Immunol.* **11**, 42 (2020).
27. Constantinides, M. G. et al. MAIT cells are imprinted by the microbiota in early life and promote tissue repair. *Science* **366**, eaax6624 (2019).
28. Yan, J. et al. MAIT cells promote tumor initiation, growth, and metastases via tumor MR1. *Cancer Discov.* **10**, 124–141 (2020).
29. Rochman, Y., Spolski, R. & Leonard, W. J. New insights into the regulation of T cells by γc family cytokines. *Nat. Rev. Immunol.* **9**, 480–490 (2009).
30. Webster, K. E. et al. IL-17-producing NKT cells depend exclusively on IL-7 for homeostasis and survival. *Mucosal Immunol.* **7**, 1058–1067 (2014).
31. Corpuz, T. M. et al. Differential Responsiveness of Innate-like IL-17- and IFN-gamma-Producing γδ T cells to Homeostatic cytokines. *J. Immunol.* **196**, 645–654 (2016).
32. Corpuz, T. M. et al. IL-2 Shapes the Survival and Plasticity of IL-17-Producing γδ T cells. *J. Immunol.* **199**, 2366–2376 (2017).
33. Tao, H. et al. Differential controls of MAIT cell effector polarization by mTORC1/mTORC2 via integrating cytokine and costimulatory signals. *Nat. Commun.* **12**, 2029 (2021).
34. Hassane, M. et al. Interleukin-7 protects against bacterial respiratory infection by promoting IL-17A-producing innate T-cell response. *Mucosal Immunol.* **13**, 128–139 (2020).
35. Bedel, R. et al. Lower TCR repertoire diversity in Traj18-deficient mice. *Nat. Immunol.* **13**, 705–706 (2012).
36. Rahimpour, A. et al. Identification of phenotypically and functionally heterogeneous mouse mucosal-associated invariant T cells using MR1 tetramers. *J. Exp. Med.* **212**, 1095–1108 (2015).
37. Lee, Y. J., Holzapfel, K. L., Zhu, J., Jameson, S. C. & Hogquist, K. A. Steady-state production of IL-4 modulates immunity in mouse strains and is determined by lineage diversity of iNKT cells. *Nat. Immunol.* **14**, 1146–1154 (2013).
38. Dai, H. et al. Syndecan-1 identifies and controls the frequency of IL-17-producing naive natural killer T (NKT17) cells in mice. *Eur. J. Immunol.* **45**, 3045–3051 (2015).
39. Itohara, S. et al. T cell receptor delta gene mutant mice: independent generation of alpha beta T cells and programmed rearrangements of gamma delta TCR genes. *Cell* **72**, 337–348 (1993).
40. Carico, Z. & Krangel, M. S. Chromatin dynamics and the development of the TCRalpha and TCRdelta repertoires. *Adv. Immunol.* **128**, 307–361 (2015).
41. Cui, Y. et al. Mucosal-associated invariant T cell-rich congenic mouse strain allows functional evaluation. *J. Clin. Invest.* **125**, 4171–4185 (2015).
42. Bosc, N. & Lefranc, M. P. The mouse (Mus musculus) T cell receptor alpha (TRA) and delta (TRD) variable genes. *Dev. Comp. Immunol.* **27**, 465–497 (2003).

43. Carico, Z. M., Roy Choudhury, K., Zhang, B., Zhuang, Y. & Krangel, M. S. Tcrd rearrangement redirects a processive Tcra recombination program to expand the Tcra repertoire. *Cell Rep.* **19**, 2157–2173 (2017).
44. Hamrouni, A., Olsson, A., Wiegers, G. J. & Villunger, A. Impact of cellular lifespan on the T cell receptor repertoire. *Eur. J. Immunol.* **37**, 1978–1985 (2007).
45. Ogilvy, S. et al. Constitutive Bcl-2 expression throughout the hematopoietic compartment affects multiple lineages and enhances progenitor cell survival. *Proc. Natl Acad. Sci. U. S. A.* **96**, 14943–14948 (1999).
46. Matsuda, J. L. et al. Homeostasis of V alpha 14i NKT cells. *Nat. Immunol.* **3**, 966–974 (2002).
47. Gherardin, N. A. et al. Human blood MAIT cell subsets defined using MR1 tetramers. *Immunol. Cell Biol.* **96**, 507–525 (2018).
48. Binz, C., Bubke, A., Sandrock, I. & Prinz, I. αβ T cells replacing dermal and epidermal γδ T cells in Tcrd−/− mice express an MHC-independent TCR repertoire. *Eur. J. Immunol.* **51**, 2618–2632 (2021).
49. Ataide, M. A. et al. Lymphatic migration of unconventional T cells promotes site-specific immunity in distinct lymph nodes. *Immunity* **55**, 1813–1828.e9 (2022).
50. Michel, M. L. et al. Interleukin 7 (IL-7) selectively promotes mouse and human IL-17-producing gammadelta cells. *Proc. Natl Acad. Sci. U. S. A.* **109**, 17549–17554 (2012). https://doi.org/10.1073/pnas.1204327109.
51. Baccala, R. et al. γδ T cell Homeostasis Is Controlled by IL-7 and IL-15 Together with Subset-Specific Factors. *J. Immunol.* **174**, 4606–4612 (2005). https://doi.org/10.4049/jimmunol.174.8.4606.
52. Lockhart, E., Green, A. M. & Flynn, J. L. IL-17 Production Is Dominated by γδ T cells rather than CD4 T cells during Mycobacterium tuberculosis Infection. *J. Immunol.* **177**, 4662–4669 (2006). https://doi.org/10.4049/jimmunol.177.7.4662.
53. Doisne, J. M. et al. Cutting edge: crucial role of IL-1 and IL-23 in the innate IL-17 response of peripheral lymph node NK1.1- invariant NKT cells to bacteria. *J. Immunol.* **186**, 662–666 (2011). https://doi.org/10.4049/jimmunol.1002725.
54. Tao, H. et al. Thymic epithelial cell-Derived IL-15 and IL-15 Receptor alpha Chain Foster Local Environment for Type 1 Innate Like T cell Development. *Front. Immunol.* **12**:. https://doi.org/10.3389/fimmu.2021.623280623280.
55. Ranson, T. et al. IL-15 availability conditions homeostasis of peripheral natural killer T cells. *Proc. Natl Acad. Sci. USA* **100**, 2663–2668 (2003). https://doi.org/10.1073/pnas.0535482100.
56. Gordy, L. E. et al. IL-15 regulates homeostasis and terminal maturation of NKT cells. *J. Immunol.* **187**, 6335–6345 (2011). https://doi.org/10.4049/jimmunol.1003965.
57. Matsuda, J. L. et al. Tracking the response of natural killer T cells to a glycolipid antigen using CD1d tetramers. *J. Exp. Med.* **192**, 741–754 (2000). https://doi.org/10.1084/jem.192.5.741.
58. Takagaki, Y., DeCloux, A., Bonneville, M. & Tonegawa, S. Diversity of gamma Delta T-cell receptors on murine intestinal intra-epithelial lymphocytes. *Nature* **339**, 712–714 (1989). https://doi.org/10.1038/339712a0.
59. Borges Da Silva, H., Wang, H., Qian, L. J., Hogquist, K. A. & Jameson, S. C. ARTC2.2/P2RX7 signaling during cell isolation distorts function and quantification of tissue-resident CD8+ T cell and invariant NKT subsets. *J. Immunol.* **202**, 2153–2163 (2019).
60. Lin, Q., Kuypers, M., Philpott, D. J. & Mallevaey, T. The dialogue between unconventional T cells and the microbiota. *Mucosal Immunol.* **13**, 867–876 (2020).
61. Leinwand, J. C. et al. Intrahepatic microbes govern liver immunity by programming NKT cells. *J. Clin. Invest.* **132**, e151725 (2022).
62. Lett, M. J. et al. Stimulatory MAIT cell antigens reach the circulation and are efficiently metabolised and presented by human liver cells. *Gut* **71**, 2526–2538 (2022).
63. Legoux, F. et al. Microbial metabolites control the thymic development of mucosal-associated invariant T cells. *Science* **366**, 494–499 (2019).
64. Dashtsoodol, N. et al. Generation of novel Traj18-deficient mice lacking Vα14 natural killer T cells with an undisturbed T cell receptor α-chain repertoire. *PLoS One* **11**, e0153347 (2016).
65. Xie, J. et al. Deficiency of mucosal-associated invariant T cells in TCRJα18 germline knockout mice. *Immunohorizons* **3**, 203–207 (2019).
66. Chen, Z. et al. Characterization and purification of mouse mucosal-associated invariant T (MAIT) cells. *Curr. Protoc. Immunol.* **127**, e89 (2019).
67. Chen, Z. et al. Mucosal-associated invariant T-cell activation and accumulation after in vivo infection depends on microbial riboflavin synthesis and co-stimulatory signals. *Mucosal Immunol.* **10**, 58–68 (2017).
68. Wang, H. et al. MAIT cells protect against pulmonary Legionella longbeachae infection. *Nat. Commun.* **9**, 3350 (2018).
69. Leeansyah, E. et al. Arming of MAIT cell cytolytic antimicrobial activity is induced by IL-7 and defective in HIV-1 infection. *PLoS Pathog.* **11**, e1005072 (2015).
70. Walker, L. J. et al. Human MAIT and CD8αα cells develop from a pool of type-17 precommitted CD8+ T cells. *Blood* **119**, 422–433 (2012).
71. Lu, B. et al. IL-17 production by tissue-resident MAIT cells is locally induced in children with pneumonia. *Mucosal Immunol.* **13**, 824–835 (2020).
72. Gibbs, A. et al. MAIT cells reside in the female genital mucosa and are biased towards IL-17 and IL-22 production in response to bacterial stimulation. *Mucosal Immunol.* **10**, 35–45 (2017).
73. Chandra, S. et al. Transcriptomes and metabolism define mouse and human MAIT cell heterogeneity. bioRxiv, Available at: https://doi.org:10.1101/2021.12.20.473182 (2021) [Date accessed: 13 MARCH 2022].
74. Ben Youssef, G. et al. Ontogeny of human mucosal-associated invariant T cells and related T cell subsets. *J. Exp. Med.* **215**, 459–479 (2018).
75. Howson, L. J. et al. Absence of mucosal-associated invariant T cells in a person with a homozygous point mutation in MR1. *Sci. Immunol.* **5**, eabc9492 (2020).
76. Mayassi, T., Barreiro, L. B., Rossjohn, J. & Jabri, B. A multilayered immune system through the lens of unconventional T cells. *Nature* **595**, 501–510 (2021).
77. Godfrey, D. I., Le Nours, J., Andrews, D. M., Uldrich, A. P. & Rossjohn, J. Unconventional T cell targets for cancer immunotherapy. *Immunity* **48**, 453–473 (2018).
78. Yang, H., Wang, H. & Jaenisch, R. Generating genetically modified mice using CRISPR/Cas-mediated genome engineering. *Nat. Protoc.* **9**, 1956–1968 (2014).
79. Smiley, S. T., Kaplan, M. H. & Grusby, M. J. Immunoglobulin E production in the absence of interleukin-4-secreting CD1-dependent cells. *Science* **275**, 977–979 (1997).
80. Sonoda, K. H., Exley, M., Snapper, S., Balk, S. P. & Stein-Streilein, J. CD1-reactive natural killer T cells are required for development of systemic tolerance through an immune-privileged site. *J. Exp. Med.* **190**, 1215–1226 (1999).
81. Corbett, A. J. et al. T-cell activation by transitory neo-antigens derived from distinct microbial pathways. *Nature* **509**, 361–365 (2014).
82. Eckle, S. B. et al. A molecular basis underpinning the T cell receptor heterogeneity of mucosal-associated invariant T cells. *J. Exp. Med.* **211**, 1585–1600 (2014).
83. Pellicci, D. G. et al. Differential recognition of CD1d-alpha-galactosyl ceramide by the V beta 8.2 and V beta 7 semi-invariant NKT T cell receptors. *Immunity* **31**, 47–59 (2009).
84. Pfaffl, M. W. A new mathematical model for relative quantification in real-time RT-PCR. *Nucleic Acids Res.* **29**, e45 (2001).
85. Tilloy, F. et al. An invariant T cell receptor alpha chain defines a novel TAP-independent major histocompatibility complex class Ib-restricted alpha/beta T cell subpopulation in mammals. *J. Exp. Med.* **189**, 1907–1921 (1999).
86. Medrano, G., Guan, P., Barlow-Anacker, A. J. & Gosain, A. Comprehensive selection of reference genes for quantitative RT-PCR analysis of murine extramedullary hematopoiesis during development. *PLoS One* **12**, e0181881 (2017).
87. Guangwei, C., Takahiro, H., Szandor, S., Keisuke, W., Akifumi, A., Hitoshi, M., Satsuki, K., Masaru, I., Shizue, T. & Koichi, I. Characterization of the IL-15 niche in primary and secondary lymphoid organs in vivo. *Proc Natl Acad Sci U S A.* **111** (5), 1915–1920 (2014).
88. Christopher, E. M., Darina, S. S., Kwesi, F.-B., Hee-Ok, K., Minji, L., Kwang, S. K. & Charles, D. S. Interleukin-7 Availability Is Maintained by a Hematopoietic Cytokine Sink Comprising Innate Lymphoid Cells and T Cells. *Immunity.* **47**(1), 171–182 (2017).
89. Waskom, M. Seaborn: statistical data visualization. *J. Open Source Softw.* **6**, 3021 (2021).
90. Rissiek, B., Danquah, W., Haag, F. & Koch-Nolte, F. Technical Advance: A new cell preparation strategy that greatly improves the yield of vital and functional Tregs and NKT cells. *J. Leukoc. Biol.* **95**, 543–549 (2014).